https://doi.org/10.3311/PPci.42366



Periodica Polytechnica Civil Engineering

# Simplified Analysis of Tall Buildings for Soil–structure Interaction in Uniform and Non-uniform Buildings

Mao Cristian Pinto-Cruz[1,2*]

[1] Department of Civil and Environmental Engineering, Pontifical Catholic University of Rio de Janeiro, Rua Marquês de São Vicente 225., 22451-900 Rio de Janeiro, Brazil
[2] Department of Civil Engineering, National University of Engineering, Avenue Túpac Amaru 210., 15333 Lima, Peru
[*] Corresponding author, e-mail: mao.pinto.c@uni.pe

Received: 30 September 2025, Accepted: 18 December 2025, Published online: 20 January 2026

**Abstract**

This paper presents a continuous analytical model for evaluating the static and dynamic response of tall buildings considering soil–structure interaction. The structure is represented as a parallel coupling of a bending beam and a shear beam, connected by rigid horizontal links, and supported by translational and rotational springs that account for foundation flexibility. The governing equations are derived via Hamilton's principle, explicitly including both translational and rotational inertias. For buildings with uniform properties, closed-form solutions are obtained using the Laplace transform. To extend the formulation to non-uniform buildings, a modified transfer matrix method is introduced that avoids matrix inversion, thereby reducing computational cost. Parametric studies highlight the sensitivity of natural frequencies to soil flexibility and demonstrate the influence of rotational inertia on higher vibration modes, which is often neglected in previous studies. The formulation is restricted to the linear elastic range and does not incorporate second-order ($P$–$\Delta$) effects or material plasticity, thereby delineating its applicability to structures without significant geometric or material nonlinearities. Numerical comparisons with finite element results confirm the accuracy and efficiency of the proposed approach, providing a practical tool for the preliminary design and performance assessment of tall buildings on flexible foundations.

**Keywords**

static and dynamic analysis, transfer matrix method, rotational inertia, soil–structure interaction, tall buildings

## 1 Introduction

Contemporary finite element (FEM) software packages allow engineers to perform highly detailed and rigorous structural analyses of tall buildings. However, the use of refined meshes significantly increases the number of degrees of freedom, which in turn leads to high computational costs and potentially impractical runtimes, particularly during the preliminary design stage. In contrast, continuous analytical models, based on equivalent stiffness parameters and generalized kinematic fields, offer a powerful alternative. Such models drastically reduce the dimensionality of the system while retaining the ability to capture the dominant global structural behaviors. This reduction not only enhances computational efficiency but also facilitates the identification and physical interpretation of the most influential structural mechanisms.

The use of continuous models to characterize the behavior of tall buildings dates back to the pioneering work of Jacobsen [1], who represented the supporting soil as a shear beam in the 1930s. Building upon this idea, Biot [2] extended the approach to investigate the seismic response of building structures. A major step forward was introduced by Chitty [3], who proposed a cantilever beam composed of parallel bending and shear beams interconnected by rigid, axially inextensible links, thereby establishing a continuous model capable of representing both bending and shear deformations. This formulation was subsequently applied by Chitty and Wan [4] to the static analysis of tall buildings; however, axial deformations in vertical elements were neglected, which constitutes a significant limitation for tall building systems. In the decades that followed, numerous studies expanded these concepts to encompass a wide range of structural configurations and boundary conditions, including contributions by Skattum [5], Rosman [6, 7], Hegedűs and Kollár [8], Miranda [9], Potzta and Kollár [10], Zalka [11], Bozdogan et al. [12], Bozdogan and Ozturk [13], Bozdogan [14, 15],

**Cite this article as:** Pinto-Cruz, M. C. "Simplified Analysis of Tall Buildings for Soil–structure Interaction in Uniform and Non-uniform Buildings", Periodica Polytechnica Civil Engineering, 2026. https://doi.org/10.3311/PPci.42366

Catal [16], Chesnais et al. [17], Zalka [18], Capsoni and Moghadasi Faridani [19], Wang et al. [20], Laier [21], and Franco et al. [22].

Early analytical models were generally based on single-field formulations such as the classical Euler–Bernoulli bending beam or the shear beam. These models were capable of capturing global bending and shear behavior but neglected axial deformations in vertical members. Over time, two-field models gained wider acceptance. The Timoshenko beam, which combines bending and shear effects in series, became a standard tool for capturing the interaction between bending and shear deformations. In parallel, sandwich beam formulations—consisting of a Timoshenko beam coupled with a bending beam—were proposed to enrich the representation of deformation mechanisms. More recently, multi-field models have been introduced to further enhance accuracy. The generalized sandwich beam and its modified variants, for instance, explicitly account for local shear mechanisms in structural walls [17, 19]. Although often overlooked in earlier studies, these mechanisms have been shown to significantly influence the dynamic response of tall buildings.

The study of soil–structure interaction (SSI) has been dominated by numerical approaches, including the finite element method, the finite difference method, and the boundary element method. While these techniques offer high fidelity, they require significant computational resources and are therefore less suitable for rapid preliminary analyses. Continuous analytical models, on the other hand, have traditionally assumed rigid-base conditions and have thus neglected foundation flexibility. Two main strategies are commonly used for SSI modeling: the direct method, in which the soil and the structure are modeled as a unified finite element domain, and the substructure method, in which the soil–foundation system and the superstructure are treated as distinct but interacting subsystems. The substructure approach, adopted in this study, offers important advantages in terms of computational efficiency and has been shown to provide sufficient accuracy for engineering practice [23–25].

Several researchers have sought to integrate SSI effects into continuous formulations. Ambrosini [23] developed a lumped-parameter model based on a generalized beam formulation to investigate the role of soil damping in seismic response. Nakhaei and Ali Ghannad [24] conducted parametric studies on nonlinear single-degree-of-freedom systems, demonstrating the influence of soil–structure stiffness ratios on seismic damage indices. Medina et al. [25] developed methods to estimate natural periods and damping ratios for pile-supported shear buildings, explicitly accounting for SSI. Other studies incorporated SSI using Timoshenko beam formulations, including those by Cheng and Heaton [26], Shirzad-Ghaleroudkhani et al. [27], Taciroglu et al. [28], Di and Fu [29], and Kara et al. [30]. Hybrid approaches have also emerged, such as optimization-based formulations aimed at reducing seismic demands [31], boundary-element/continuous-beam couplings [32], Bayesian system identification techniques [33, 34], and equivalent discrete–continuous models for control systems [35–37]. Additional studies have examined higher-mode effects under SSI [38], seismic wave propagation effects [39], and global buckling under soil flexibility [40]. Despite this extensive body of research, key limitations remain. Most classical continuous formulations assume constant mechanical properties along the height of the building, thereby restricting their applicability to realistic structures in which stiffness and mass vary with elevation. Similarly, foundation flexibility is often disregarded, even though it substantially modifies both static and dynamic responses. Moreover, rotational inertia is usually neglected in analytical formulations, despite its growing influence on higher vibration modes.

Although several studies have advanced continuous formulations in different directions—including soil–structure interaction (e.g., Ambrosini [23]; Medina et al. [25]; Taciroglu et al. [28]), generalized continua and multi-field models for wall–frame systems (Chesnais et al. [17]; Capsoni and Moghadasi Faridani [19]), and the influence of rotational inertia on higher vibration modes (Tong and Christopoulos [38])—these contributions typically address these aspects in isolation. Only a limited number of works incorporate foundation flexibility, rotational inertia, and height-varying properties simultaneously within a unified continuous beam analogy. This gap motivates the development of the present formulation, which integrates these effects in a consistent manner and provides a computationally efficient framework suitable for both uniform and non-uniform tall buildings.

In this study, a continuous model is developed based on the parallel coupling of a bending beam and a shear beam, which is extended to explicitly incorporate soil flexibility and rotational inertia. The governing equations, constitutive relations, and boundary conditions are derived rigorously using Hamilton's principle. Closed-form solutions are obtained for uniform buildings through the Laplace transform, while a modified transfer matrix method is introduced for non-uniform structures. This formulation

avoids matrix inversion, thereby improving computational efficiency. Parametric investigations are conducted to assess the influence of soil flexibility, stiffness distribution, and rotational inertia on both static and dynamic responses. Comparisons with reference models and finite element simulations confirm the accuracy of the proposed formulation, demonstrating its potential as a practical tool for the preliminary design and assessment of tall buildings considering soil–structure interaction.

## 2 Continuous model: parallel coupling of a bending beam and a shear beam

The tall building is represented by a continuous model obtained from the parallel coupling of a bending beam (hereafter, EBB beam) and a shear beam (hereafter, SB beam). This formulation, originally proposed by Chitty [3] and Chitty and Wan [4], is herein referred to as the coupled shear–bending beam (hereafter, CTB beam). The two beams are interconnected by rigid, axially inextensible horizontal links that transmit only horizontal forces without undergoing deformation (Fig. 1).

The EBB beam is responsible for resisting bending deformations, whereas the SB beam resists shear deformations. By enforcing equal horizontal displacements through rigid connectors, the system combines the complementary deformation profiles of both components. Specifically, the EBB beam exhibits a deformation shape favorable to lateral loading, with a maximum slope at the base, whereas the SB beam displays a profile with a maximum slope at the top. Their parallel coupling generates a hybrid deformation mode: bending-dominated in the lower stories—thereby limiting displacements near the base—and shear-dominated in the upper stories—thereby reducing displacements at the top. This interaction enhances the overall lateral stiffness of the structure, often exceeding the sum of the individual stiffnesses of the two beams.

The CTB beam is described by a single transverse displacement field, denoted as $u(z)$, which is shared by both sub-beams through the rigid links. The bending and shear stiffnesses are denoted by $K_b$ and $K_s$, respectively, and the total height of the building is denoted by $H$. Soil flexibility is modeled through translational and rotational springs characterized by stiffnesses $K_T$ and $K_R$, respectively.

The following assumptions are adopted:

1. structural elements behave in a linear elastic manner;
2. diaphragms are considered rigid in their plane and transmit only horizontal forces;
3. axial deformations in vertical elements are neglected;
4. discrete shear forces transmitted by the connectors are modeled as a continuous shear flow at the midplane of the connecting elements;
5. the Bernoulli–Navier hypothesis applies to the connecting beams;
6. second-order ($P$–$\Delta$) effects are neglected; and
7. connecting beams do not undergo axial deformations.

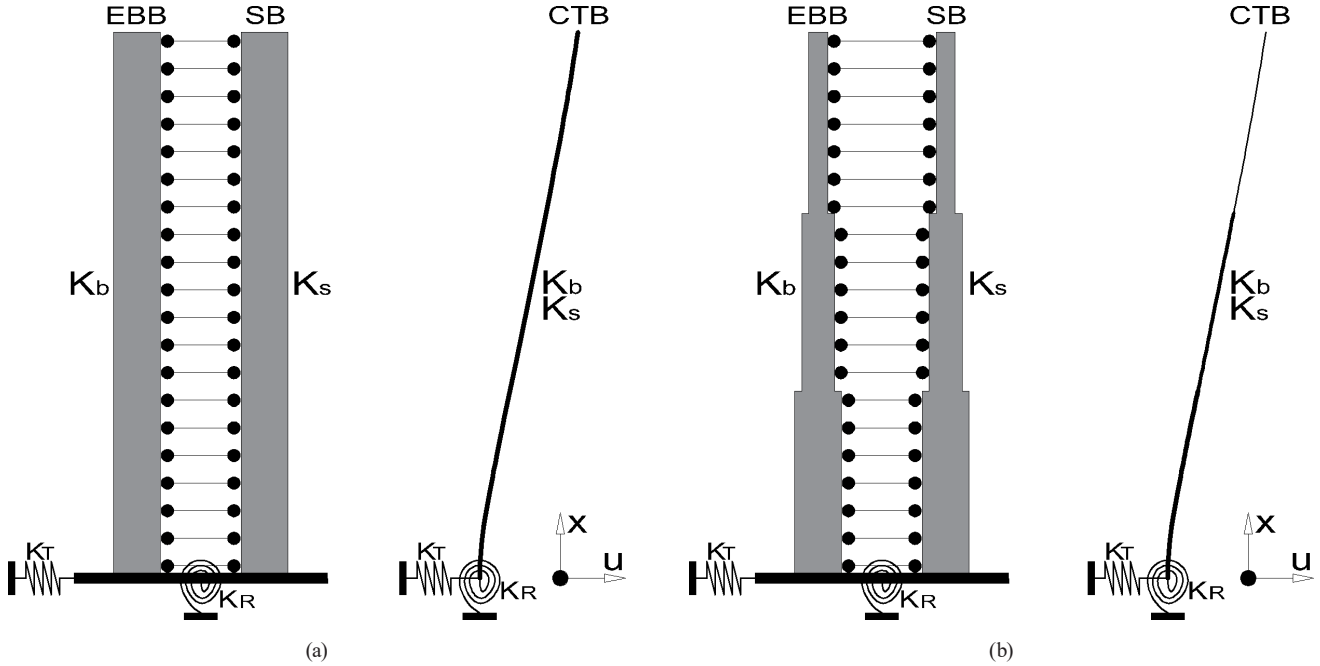


**Fig. 1** CTB beam with flexible base support: (a) uniform properties, (b) variable properties

It should be noted that the formulation developed in this study is restricted to the linear elastic range and does not incorporate *P*–Δ effects or global instability phenomena. Although these effects may become relevant in tall buildings subjected to severe seismic actions, their inclusion would require extending the analysis to a geometrically nonlinear framework, which lies beyond the scope of the present work. Consequently, the proposed model is applicable to structures in which lateral drifts remain moderate, a condition typically satisfied by buildings with sufficient lateral stiffness and moderate seismic demands.

## 3 Static analysis

### 3.1 Governing equations and boundary conditions

The strain energy of the CTB beam is expressed as:

$$\Xi = \frac{1}{2}\int_0^H K_b\left[u''(x)\right]^2 dx + \frac{1}{2}\int_0^H K_s\left[u'(x)\right]^2 dx + \frac{1}{2}K_T\left[u(0)\right]^2 + \frac{1}{2}K_R\left[u'(0)\right]^2 \tag{1}$$

The work done by an arbitrary distributed lateral force $f(x)$ along the height is:

$$W = \int_0^H f(x)u(x)dx \tag{2}$$

Therefore, the Lagrangian functional is expressed as:

$$\Pi = \frac{1}{2}\int_0^H K_b\left[u''(x)\right]^2 dx + \frac{1}{2}\int_0^H K_s\left[u'(x)\right]^2 dx + \frac{1}{2}K_T\left[u(0)\right]^2 + \frac{1}{2}K_R\left[u'(0)\right]^2 - \int_0^H f(x)u(x)dx \tag{3}$$

According to Hamilton's principle:

$$\delta\int_{t_1}^{t_2}(\Xi - W)dt = \delta\int_{t_1}^{t_2}\Pi dt = 0 \tag{4}$$

Substituting Eq. (3) into Eq. (4) and integrating by parts yields the governing equilibrium equation:

$$K_b u''''(x) - K_s u''(x) - f(x) = 0 \tag{5}$$

Constitutive laws (moment and shear force):

$$M(x) = K_b u''(x) \tag{6}$$

$$V(x) = -K_b u'''(x) + K_s u'(x) \tag{7}$$

Boundary conditions:

- At the clamped end (base)

$$u(0) = \frac{V(0)}{K_T} \tag{8}$$

$$u'(0) = \frac{M(0)}{K_R} \tag{9}$$

- At the free end (top)

$$M(H) = 0 \tag{10}$$

$$V(H) = 0 \tag{11}$$

It is worth noting that, since the static problem does not involve kinetic energy, the governing equation can be derived directly from the principle of minimum potential energy. The use of Hamilton's principle in Eq. (4) is equivalent in this context and is retained solely for consistency with the variational framework adopted later in the dynamic formulation.

### 3.2 Analytical and numerical formulation

To facilitate analysis, the governing equation is normalized with respect to the dimensionless coordinate $z = x/H$:

$$u''''(z) - \frac{K_s H^2}{K_b}u''(z) = \frac{H^4}{K_b}f(z) \tag{12}$$

The normalized internal forces are expressed as:

$$M^*(z) = \frac{H^2}{K_b}M(z) = u''(z) \tag{13}$$

$$V^*(z) = \frac{H^3}{K_b}V(z) = -u'''(z) + \alpha^2 u'(z) \tag{14}$$

A key dimensionless parameter, denoted as the lateral stiffness ratio or coupling factor, is defined as:

$$\alpha = H\sqrt{\frac{K_s}{K_b}} \tag{15}$$

This ratio controls the relative contributions of shear and bending deformations. When $\alpha \to 0$, the model reduces to a pure bending beam (EBB). When $\alpha \to \infty$, the model approaches pure shear (SB). Intermediate values capture the coupled behavior [9].

Substituting these definitions, the normalized governing equation becomes:

$$u''''(z) - \alpha^2 u''(z) = \lambda(z) \tag{16}$$

Assuming that $u(z)$ is defined for $z > 0$, its Laplace transform is defined as:

$$U(s) = L\left[u(z)\right] = \int_0^\infty u(z) e^{-sz} dz \tag{17}$$

Applying the Laplace transform to the governing equation yields:

$$U(s) = \frac{1}{s}u(0) + \frac{1}{s^2-\alpha^2}u'(0) + \frac{1}{s\left(s^2-\alpha^2\right)}M^*(0) - \frac{1}{s^2\left(s^2-\alpha^2\right)}V^*(0) + \frac{1}{s^2\left(s^2-\alpha^2\right)}L\left[\lambda(z)\right] \tag{18}$$

The application of the Laplace transform allows the differential equation to be solved in a more convenient transformed domain. Subsequently, the inverse Laplace transform is applied to project the solution back into the original physical space. The contribution of the lateral load $f(z)$ is evaluated using the convolution theorem. Applying this procedure yields:

$$\begin{aligned} u(z) &= u(0) + \frac{\sinh(\alpha z)}{\alpha}u'(0) + \frac{-1+\cosh(\alpha z)}{\alpha^2}M^*(0) + \frac{(\alpha z)-\sinh(\alpha z)}{\alpha^3}V^*(0) \\ &+ \int_0^z \lambda(\tau)\left[\frac{-(\alpha(z-\tau)) + \sinh(\alpha(z-\tau))}{\alpha^3}\right]d\tau \end{aligned} \tag{19}$$

$$u'(z) = \cosh(\alpha z)u'(0) + \frac{\sinh(\alpha z)}{\alpha}M^*(0) + \frac{1-\cosh(\alpha z)}{\alpha^2}V^*(0) + \int_0^z \lambda(\tau)\left[\frac{-1+\cosh(\alpha(z-\tau))}{\alpha^2}\right]d\tau \tag{20}$$

The internal forces are expressed as:

$$M^*(z) = \alpha\sinh(\alpha z)u'(0) + \cosh(\alpha z)M^*(0) + \frac{-\sinh(\alpha z)}{\alpha}V^*(0) + \int_0^z \lambda(\tau)\left[\frac{\sinh(\alpha(z-\tau))}{\alpha}\right]d\tau \tag{21}$$

$$V^*(z) = V^*(0) - \int_0^z \lambda(\tau)\,d\tau \tag{22}$$

The displacement and internal force vectors can then be assembled in compact matrix form:

$$\begin{Bmatrix} u(z) \\ u'(z) \\ M^*(z) \\ V^*(z) \end{Bmatrix} = \begin{bmatrix} 1 & \frac{\sinh(\alpha z)}{\alpha} & \frac{-1+\cosh(\alpha z)}{\alpha^2} & \frac{(\alpha z)-\sinh(\alpha z)}{\alpha^3} \\ 0 & \cosh(\alpha z) & \frac{\sinh(\alpha z)}{\alpha} & \frac{1-\cosh(\alpha z)}{\alpha^2} \\ 0 & \alpha\sinh(\alpha z) & \cosh(\alpha z) & -\frac{\sinh(\alpha z)}{\alpha} \\ 0 & 0 & 0 & 1 \end{bmatrix} \begin{Bmatrix} u(0) \\ u'(0) \\ M^*(0) \\ V^*(0) \end{Bmatrix} + \begin{Bmatrix} \int_0^z \lambda(\tau)\left[\frac{-(\alpha(z-\tau)) + \sinh(\alpha(z-\tau))}{\alpha^3}\right]d\tau \\ \int_0^z \lambda(\tau)\left[\frac{-1+\cosh(\alpha(z-\tau))}{\alpha^2}\right]d\tau \\ \int_0^z \lambda(\tau)\left[\frac{\sinh(\alpha(z-\tau))}{\alpha}\right]d\tau \\ -\int_0^z \lambda(\tau)\,d\tau \end{Bmatrix} \tag{23}$$

or

$$\begin{Bmatrix} u(z) \\ u'(z) \\ M^*(z) \\ V^*(z) \end{Bmatrix} = \begin{bmatrix} 1 & \frac{\sinh(\alpha z)}{\alpha} & \frac{-1+\cosh(\alpha z)}{\alpha^2} & \frac{(\alpha z)-\sinh(\alpha z)}{\alpha^3} \\ 0 & \cosh(\alpha z) & \frac{\sinh(\alpha z)}{\alpha} & \frac{1-\cosh(\alpha z)}{\alpha^2} \\ 0 & \alpha\sinh(\alpha z) & \cosh(\alpha z) & -\frac{\sinh(\alpha z)}{\alpha} \\ 0 & 0 & 0 & 1 \end{bmatrix} \begin{Bmatrix} u(0) \\ u'(0) \\ \frac{u'(0)}{\beta_R^2} \\ \frac{u(0)}{\beta_T^2} \end{Bmatrix} + \begin{Bmatrix} \int_0^z \lambda(\tau)\left[\frac{-(\alpha(z-\tau))+\sinh(\alpha(z-\tau))}{\alpha^3}\right]d\tau \\ \int_0^z \lambda(\tau)\left[\frac{-1+\cosh(\alpha(z-\tau))}{\alpha^2}\right]d\tau \\ \int_0^z \lambda(\tau)\left[\frac{\sinh(\alpha(z-\tau))}{\alpha}\right]d\tau \\ -\int_0^z \lambda(\tau)\,d\tau \end{Bmatrix} \tag{24}$$

where $\beta_T$ and $\beta_R$ are two additional parameters that represent the soil flexibility:

$$\beta_T^2 = \frac{K_b}{H^3 K_T} \tag{25}$$

$$\beta_R^2 = \frac{K_b}{H^2 K_R} \tag{26}$$

Applying the boundary conditions and solving yields:

$$u(0) = \beta_T^2 \int_0^1 \lambda(\tau)\,d\tau \tag{27}$$

$$u'(0) = \beta_R^2 \frac{-\int_0^1 \lambda(\tau)\sinh(\alpha(z-\tau))\,d\tau + \sinh(\alpha)\int_0^1 \lambda(\tau)\,d\tau}{\alpha\left[\beta_R^2\alpha\sinh(\alpha)+\cosh(\alpha)\right]} \tag{28}$$

Given $u(0)$ and $u'(0)$, the displacement and internal force fields are determined analytically. Furthermore, the transfer matrix is obtained directly:

$$M(z) = \begin{bmatrix} 1 & \frac{\sinh(\alpha z)}{\alpha} & \frac{-1+\cosh(\alpha z)}{\alpha^2} & \frac{(\alpha z)-\sinh(\alpha z)}{\alpha^3} \\ 0 & \cosh(\alpha z) & \frac{\sinh(\alpha z)}{\alpha} & \frac{1-\cosh(\alpha z)}{\alpha^2} \\ 0 & \alpha\sinh(\alpha z) & \cosh(\alpha z) & -\frac{\sinh(\alpha z)}{\alpha} \\ 0 & 0 & 0 & 1 \end{bmatrix} \tag{29}$$

The relationship between displacement and internal force vectors across consecutive stories is expressed as:

$$\begin{Bmatrix} u \\ u' \\ M^* \\ V^* \end{Bmatrix}_{i+1} = \boldsymbol{M}_i \begin{Bmatrix} u \\ u' \\ M^* \\ V^* \end{Bmatrix}_i + \boldsymbol{F}_i \tag{30}$$

where $\boldsymbol{F}_i$ is the lateral load vector applied at the $i$-th node.

The relationship between the force–displacement vectors at the $n$-th and initial stories is established by multiplying the transfer matrices and incorporating the external force vector [12]:

$$\begin{Bmatrix} u \\ u' \\ M^* \\ V^* \end{Bmatrix}_n = \prod_{k=n}^{1} \boldsymbol{M}_k \begin{Bmatrix} u(0) \\ u'(0) \\ M^*(0) \\ V^*(0) \end{Bmatrix}_1 + \sum_{s=1}^{n-1}\left[\prod_{k=n}^{s+1} \boldsymbol{M}_k\right]\boldsymbol{F}_s + \boldsymbol{F}_n \tag{31}$$

i.e.,

$$\begin{Bmatrix} u \\ u' \\ M^* \\ V^* \end{Bmatrix}_n = \boldsymbol{N} \begin{Bmatrix} u(0) \\ u'(0) \\ M^*(0) \\ V^*(0) \end{Bmatrix}_1 + \boldsymbol{f} \tag{32}$$

where [12–15]

$$\boldsymbol{N} = \prod_{k=n}^{1} \boldsymbol{M}_k \tag{33}$$

$$\boldsymbol{f} = \sum_{s=1}^{n-1} \left[ \prod_{k=n}^{s+1} \boldsymbol{M}_k \right] \boldsymbol{F}_s + \boldsymbol{F}_n \tag{34}$$

In simplified form [12], and substituting the boundary conditions, the expression becomes:

$$\begin{Bmatrix} u(h_n) \\ u'(h_n) \\ 0 \\ 0 \end{Bmatrix} = \begin{bmatrix} N_{1,1} & N_{1,2} & N_{1,3} & N_{1,4} \\ N_{2,1} & N_{2,2} & N_{2,3} & N_{2,4} \\ N_{3,1} & N_{3,2} & N_{3,3} & N_{3,4} \\ N_{4,1} & N_{4,2} & N_{4,3} & N_{4,4} \end{bmatrix} \begin{Bmatrix} u(0) \\ u'(0) \\ \dfrac{u'(0)}{\beta_R^2} \\ \dfrac{u(0)}{\beta_T^2} \end{Bmatrix} + \begin{Bmatrix} f_1 \\ f_2 \\ f_3 \\ f_4 \end{Bmatrix} \tag{35}$$

The displacement field is obtained by solving the resulting system of equations:

$$\begin{Bmatrix} u_n(h_n) \\ u_n'(h_n) \end{Bmatrix} = -\begin{bmatrix} N_{1,1} + \dfrac{N_{1,4}}{\beta_T^2} & N_{1,2} + \dfrac{N_{1,3}}{\beta_R^2} \\ N_{2,1} + \dfrac{N_{2,4}}{\beta_T^2} & N_{2,2} + \dfrac{N_{2,3}}{\beta_R^2} \end{bmatrix} \begin{bmatrix} N_{3,1} + \dfrac{N_{3,4}}{\beta_T^2} & N_{3,2} + \dfrac{N_{3,3}}{\beta_R^2} \\ N_{4,1} + \dfrac{N_{4,4}}{\beta_T^2} & N_{4,2} + \dfrac{N_{4,3}}{\beta_R^2} \end{bmatrix}^{-1} \begin{Bmatrix} f_3 \\ f_4 \end{Bmatrix} + \begin{Bmatrix} f_1 \\ f_2 \end{Bmatrix} \tag{36}$$

Accordingly, a general analytical solution is developed for structures with both uniform and non-uniform properties along their height, subjected to arbitrary lateral loads and variable soil flexibility. The direct derivation of the transfer matrix eliminates the need to compute the inverse of singular matrices, thereby yielding significant computational efficiency—an aspect that is particularly advantageous for tall buildings with height-dependent characteristics.

## 4 Dynamic analysis

The objective is now to derive the equations of motion of the proposed continuous model, evaluate the influence of soil–structure interaction and rotational inertia on the vibration characteristics of tall buildings, and establish a unified framework for computing natural frequencies, mode shapes, and modal responses under dynamic excitation.

### 4.1 Governing equations and boundary conditions

The strain energy of the CTB beam is expressed as:

$$\Xi = \frac{1}{2}\int_0^H K_b \left[u''(x,t)\right]^2 dx + \frac{1}{2}\int_0^H K_s \left[u'(x,t)\right]^2 dx + \frac{1}{2} K_T \left[u(0,t)\right]^2 + \frac{1}{2} K_R \left[u'(0,t)\right]^2 \tag{37}$$

The conventional coupling of bending and shear beams typically neglects rotational inertia. To explicitly include this effect, the total kinetic energy is modified as:

$$T = \frac{1}{2}\int_0^H \left[\gamma_u \dot{u}^2(x,t) + \gamma_\theta \dot{u}'^2(x,t)\right] dx \tag{38}$$

where $\gamma_u = \sum_{i=1}^{n} \rho A_i$ and $\gamma_\theta = \sum_{i=1}^{n} \rho I_i$ denote the translational and rotational mass per unit length, respectively. The prime $(\,)'$ and dot $\dot{(\,)}$ operators represent spatial and temporal derivatives, respectively.

Therefore, the Lagrangian functional is expressed as:

$$\Pi = \frac{1}{2}\int_0^H K_b \left[u''(x,t)\right]^2 dx + \frac{1}{2}\int_0^H K_s \left[u'(x,t)\right]^2 dx + \frac{1}{2} K_T \left[u(0,t)\right]^2 + \frac{1}{2} K_R \left[u'(0,t)\right]^2 - \frac{1}{2}\int_0^H \left[\gamma_u \dot{u}^2(x,t) + \gamma_\theta \dot{u}'^2(x,t)\right] dx \tag{39}$$

and Hamilton's principle requires:

$$\delta \int_{t_1}^{t_2} (\Xi - T - W)\, dt = \delta \int_{t_1}^{t_2} \Pi dt = 0 \tag{40}$$

After substitution and integration by parts, the governing equation of motion becomes:

$$\gamma_u \ddot{u}(x,t) - \gamma_\theta \ddot{u}''(x,t) + K_b u''''(x,t) - K_s u''(x,t) = 0 \tag{41}$$

Boundary conditions:

- At the clamped end (base)

$$u(0,t) = \frac{V(0,t)}{K_T} \tag{42}$$

$$u'(0,t) = \frac{M(0,t)}{K_R} \tag{43}$$

- At the free end (top)

$$M(H,t)=0 \tag{44}$$

$$V(H,t)=0 \tag{45}$$

A separation of variables is assumed:

$$u(x,t)=\phi(x)q(t) \tag{46}$$

where $\phi(z)$ is the spatial mode shape and $q(t)$ the generalized coordinate. Substituting Eq. (46) into Eq. (41) yields:

$$\ddot{q}(t)+\left[\frac{K_b\phi'''(x)-K_s\phi''(x)}{\gamma_u\phi(x)-\gamma_\theta\phi''(x)}\right]q(t)=0 \tag{47}$$

Since time and spatial coordinates are independent, each term must equal a constant with opposite signs to satisfy the identity. This leads to the decomposition of the governing equation into two ordinary differential equations.

$$\ddot{q}(t)+\omega^2 q(t)=0 \tag{48}$$

$$K_b\phi'''(x)-\left(K_s-\gamma_\theta\omega^2\right)\phi''(x)-\gamma_u\omega^2\phi(x)=0 \tag{49}$$

The first equation corresponds to the equation of motion of a single-degree-of-freedom (SDOF) system with natural frequency $\omega$.

The normalized internal forces are expressed as:

$$M^*(z)=\frac{H^2}{K_b}M(z)=\phi''(z) \tag{50}$$

$$V^*(z)=\frac{H^3}{K_b}V(z)=-\phi'''(z)+\alpha^2\phi'(z) \tag{51}$$

Three dimensionless parameters are introduced:

$$\alpha=H\sqrt{\frac{K_s}{K_b}} \tag{52}$$

$$\gamma=\sqrt{\frac{\gamma_u H^4}{K_b}\omega^2} \tag{53}$$

$$\mu=\frac{1}{H}\sqrt{\frac{\gamma_\theta}{\gamma_u}} \tag{54}$$

Normalizing with $z = x/H$:

$$\phi''''(z)-\left(\alpha^2-\gamma^2\mu^2\right)\phi''(z)-\gamma^2\phi(z)=0 \tag{55}$$

Assuming that $\phi(z)$ is defined for $z > 0$, its Laplace transform is defined as:

$$\Phi(s)=L\left[\phi(z)\right]=\int_0^\infty \phi(z)e^{-sz}dz \tag{56}$$

Applying the Laplace transform to the governing equation yields:

$$\Phi(s)=\frac{s\left[s^2-\left(\alpha^2-\gamma^2\mu^2\right)\right]}{\left(s^2-\xi^2\right)\left(s^2+\beta^2\right)}\phi(0)+\frac{s^2+\gamma^2\mu^2}{\left(s^2-\xi^2\right)\left(s^2+\beta^2\right)}\phi'(0)+\frac{s}{\left(s^2-\xi^2\right)\left(s^2+\beta^2\right)}M^*(0)-\frac{1}{\left(s^2-\xi^2\right)\left(s^2+\beta^2\right)}V^*(0) \tag{57}$$

where

$$\xi=\sqrt{\frac{\left(\alpha^2-\gamma^2\mu^2\right)+\sqrt{\left(\alpha^2-\gamma^2\mu^2\right)^2+4\gamma^2}}{2}} \tag{58}$$

$$\beta=\sqrt{\frac{-\left(\alpha^2-\gamma^2\mu^2\right)+\sqrt{\left(\alpha^2-\gamma^2\mu^2\right)^2+4\gamma^2}}{2}} \tag{59}$$

The displacements and internal forces are obtained by solving the Laplace-transformed differential equation and subsequently applying the inverse Laplace transform.

$$\begin{aligned}\phi(z)=&\left\{\frac{\left[\xi^2-\left(\alpha^2-\gamma^2\mu^2\right)\right]\cosh(\xi z)+\left[\beta^2+\left(\alpha^2-\gamma^2\mu^2\right)\right]\cos(\beta z)}{\beta^2+\xi^2}\right\}\phi(0)\\&+\left\{\frac{\left(\xi+\gamma^2\mu^2\right)\frac{\sinh(\xi z)}{\xi}+\left(\beta-\gamma^2\mu^2\right)\frac{\sin(\beta z)}{\beta}}{\beta^2+\xi^2}\right\}\phi'(0)+\left[\frac{\cosh(\xi z)-\cos(\beta z)}{\beta^2+\xi^2}\right]M^*(0)-\left[\frac{-\frac{\sinh(\xi z)}{\xi}+\frac{\sin(\beta z)}{\beta}}{\beta^2+\xi^2}\right]V^*(0)\end{aligned} \tag{60}$$

$$\phi'(z)=\left\{\frac{\left[\xi^2-\left(\alpha^2-\gamma^2\mu^2\right)\right]\xi\sinh(\xi z)-\left[\beta^2+\left(\alpha^2-\gamma^2\mu^2\right)\right]\beta\sin(\beta z)}{\beta^2+\xi^2}\right\}\phi(0)$$
$$+\left\{\frac{\left(\xi+\gamma^2\mu^2\right)\cosh(\xi z)+\left(\beta-\gamma^2\mu^2\right)\cos(\beta z)}{\beta^2+\xi^2}\right\}\phi'(0)+\left[\frac{\xi\sinh(\xi z)+\beta\sin(\beta z)}{\beta^2+\xi^2}\right]M^*(0)-\left[\frac{-\cosh(\xi z)+\cos(\beta z)}{\beta^2+\xi^2}\right]V^*(0) \tag{61}$$

$$M^*(z)=\left\{\frac{\left[\xi^2-\left(\alpha^2-\gamma^2\mu^2\right)\right]\xi^2\cosh(\xi z)-\left[\beta^2+\left(\alpha^2-\gamma^2\mu^2\right)\right]\beta^2\cos(\beta z)}{\beta^2+\xi^2}\right\}\phi(0)$$
$$+\left\{\frac{\left(\xi+\gamma^2\mu^2\right)\xi\sinh(\xi z)-\left(\beta-\gamma^2\mu^2\right)\beta\sin(\beta z)}{\beta^2+\xi^2}\right\}\phi'(0)+\left[\frac{\xi^2\cosh(\xi z)+\beta^2\cos(\beta z)}{\beta^2+\xi^2}\right]M^*(0) \tag{62}$$
$$-\left[\frac{-\xi\sinh(\xi z)-\beta\sin(\beta z)}{\beta^2+\xi^2}\right]V^*(0)$$

$$V^*(z)=\left\{\frac{-\left[\xi^2-\left(\alpha^2-\gamma^2\mu^2\right)\right]\xi\left(\xi^2-\alpha^2\right)\sinh(\xi z)-\left[\beta^2+\left(\alpha^2-\gamma^2\mu^2\right)\right]\beta\left(\beta^2+\alpha^2\right)\sin(\beta z)}{\beta^2+\xi^2}\right\}\phi(0)$$
$$+\left\{\frac{-\left(\xi+\gamma^2\mu^2\right)\left(\xi^2-\alpha^2\right)\cosh(\xi z)+\left(\beta-\gamma^2\mu^2\right)\left(\beta^2+\alpha^2\right)\cos(\beta z)}{\beta^2+\xi^2}\right\}\phi'(0) \tag{63}$$
$$+\left[\frac{-\xi\left(\xi^2-\alpha^2\right)\sinh(\xi z)+\beta\left(\beta^2+\alpha^2\right)\sin(\beta z)}{\beta^2+\xi^2}\right]M^*(0)+\left[\frac{\left(\xi^2-\alpha^2\right)\cosh(\xi z)+\left(\beta^2+\alpha^2\right)\cos(\beta z)}{\beta^2+\xi^2}\right]V^*(0)$$

The displacement and internal force vectors can then be assembled in compact matrix form:

$$\begin{Bmatrix}\phi(z)\\ \phi'(z)\\ M^*(z)\\ V^*(z)\end{Bmatrix}=\begin{bmatrix}M_{1,1}(z) & M_{1,2}(z) & M_{1,3}(z) & M_{1,4}(z)\\ M_{2,1}(z) & M_{2,2}(z) & M_{2,3}(z) & M_{2,4}(z)\\ M_{3,1}(z) & M_{3,2}(z) & M_{3,3}(z) & M_{3,4}(z)\\ M_{4,1}(z) & M_{4,2}(z) & M_{4,3}(z) & M_{4,4}(z)\end{bmatrix}\begin{Bmatrix}\phi(0)\\ \phi'(0)\\ M^*(0)\\ V^*(0)\end{Bmatrix} \tag{64}$$

i.e.,

$$\begin{Bmatrix}\phi(z)\\ \phi'(z)\\ M^*(z)\\ V^*(z)\end{Bmatrix}=\begin{bmatrix}M_{1,1}(z) & M_{1,2}(z) & M_{1,3}(z) & M_{1,4}(z)\\ M_{2,1}(z) & M_{2,2}(z) & M_{2,3}(z) & M_{2,4}(z)\\ M_{3,1}(z) & M_{3,2}(z) & M_{3,3}(z) & M_{3,4}(z)\\ M_{4,1}(z) & M_{4,2}(z) & M_{4,3}(z) & M_{4,4}(z)\end{bmatrix}\begin{Bmatrix}\phi(0)\\ \phi'(0)\\ \dfrac{\phi'(0)}{\beta_R^2}\\ \dfrac{\phi(0)}{\beta_T^2}\end{Bmatrix} \tag{65}$$

Applying the boundary conditions yields:

$$\begin{bmatrix}M_{3,1}(1)+\dfrac{M_{3,4}(1)}{\beta_T^2} & M_{3,2}(1)+\dfrac{M_{3,3}(1)}{\beta_R^2}\\ M_{4,1}(1)+\dfrac{M_{4,4}(1)}{\beta_T^2} & M_{4,2}(1)+\dfrac{M_{4,3}(1)}{\beta_R^2}\end{bmatrix}\begin{Bmatrix}\phi(z)\\ \phi'(z)\end{Bmatrix}=\begin{Bmatrix}0\\ 0\end{Bmatrix} \tag{66}$$

A non-trivial solution exists when the determinant of the coefficient matrix equals zero, indicating its singularity. After straightforward manipulations, this determinant can be expressed as:

$$\begin{aligned}&\left[M_{3,1}(1)M_{4,2}(1)-M_{3,2}(1)M_{4,1}(1)\right]\beta_T^2\beta_R^2+\left[M_{3,1}(1)M_{4,3}(1)-M_{3,3}(1)M_{4,1}(1)\right]\beta_T^2\\&+\left[M_{3,4}(1)M_{4,2}(1)-M_{3,2}(1)M_{4,4}(1)\right]\beta_R^2+\left[M_{3,4}(1)M_{4,3}(1)-M_{3,3}(1)M_{4,4}(1)\right]=0\end{aligned}\tag{67}$$

Solving the determinant yields the eigenvalues $\delta$, which in turn allow for the calculation of the vibration periods:

$$T=\frac{2\pi H^2}{r_f\gamma}\sqrt{\frac{\gamma_u}{K_b}}\tag{68}$$

where $r_f$ is a correction factor introduced to account for vertical loads applied at discrete floor levels rather than uniformly distributed along the building height [18], and $N$ denotes the number of stories.

$$r_f=\sqrt{\frac{N}{N+2.06}}\tag{69}$$

The transfer matrix is obtained as:

$$M(z)=\begin{bmatrix}M_{1,1}(z) & M_{1,2}(z) & M_{1,3}(z) & M_{1,4}(z)\\M_{2,1}(z) & M_{2,2}(z) & M_{2,3}(z) & M_{2,4}(z)\\M_{3,1}(z) & M_{3,2}(z) & M_{3,3}(z) & M_{3,4}(z)\\M_{4,1}(z) & M_{4,2}(z) & M_{4,3}(z) & M_{4,4}(z)\end{bmatrix}\tag{70}$$

The relationship between displacement and internal force vectors across consecutive stories is expressed as:

$$\begin{Bmatrix}\phi\\\phi'\\M^*\\V^*\end{Bmatrix}_i=M_i\begin{Bmatrix}\phi\\\phi'\\M^*\\V^*\end{Bmatrix}_{i-1}\tag{71}$$

The relation between forces and displacements of the $n$-th element and the initial element is established by applying the product of transfer matrices of the $n$ elements [12]:

$$\begin{Bmatrix}u_n(h_n)\\u_n'(h_n)\\M_n^*(h_n)\\V_n^*(h_n)\end{Bmatrix}_n=\prod_{k=n}^{1}M_k\begin{Bmatrix}u(0)\\u'(0)\\M^*(0)\\V^*(0)\end{Bmatrix}_1=N\begin{Bmatrix}u(0)\\u'(0)\\M^*(0)\\V^*(0)\end{Bmatrix}_1\tag{72}$$

where [12]

$$\boldsymbol{N}=\prod_{k=n}^{1}\boldsymbol{M}_k\tag{73}$$

Expressed in simplified form [12] is:

$$\begin{Bmatrix}\phi_n(h_n)\\\phi_n'(h_n)\\M_n^*(h_n)\\V_n^*(h_n)\end{Bmatrix}=\begin{bmatrix}N_{1,1} & N_{1,2} & N_{1,3} & N_{1,4}\\N_{2,1} & N_{2,2} & N_{2,3} & N_{2,4}\\N_{3,1} & N_{3,2} & N_{3,3} & N_{3,4}\\N_{4,1} & N_{4,2} & N_{4,3} & N_{4,4}\end{bmatrix}\begin{Bmatrix}\phi_1(0)\\\phi_1'(0)\\M_1^*(0)\\V_1^*(0)\end{Bmatrix}\tag{74}$$

Applying the boundary conditions yields:

$$\begin{bmatrix}N_{3,1}+\dfrac{N_{3,4}}{\beta_T^2} & N_{3,2}+\dfrac{N_{3,3}}{\beta_R^2}\\N_{4,1}+\dfrac{N_{4,4}}{\beta_T^2} & N_{4,2}+\dfrac{N_{4,3}}{\beta_R^2}\end{bmatrix}\begin{Bmatrix}\phi(z)\\\phi'(z)\end{Bmatrix}=\begin{Bmatrix}0\\0\end{Bmatrix}\tag{75}$$

A non-trivial solution exists when the determinant of the coefficient matrix vanishes, indicating singularity. The determinant can be expressed as:

$$\begin{aligned}&\left[N_{3,1}(1)N_{4,2}(1)-N_{3,2}(1)N_{4,1}(1)\right]\beta_T^2\beta_R^2+\left[N_{3,1}(1)N_{4,3}(1)-N_{3,3}(1)N_{4,1}(1)\right]\beta_T^2\\&+\left[N_{3,4}(1)N_{4,2}(1)-N_{3,2}(1)N_{4,4}(1)\right]\beta_R^2+\left[N_{3,4}(1)N_{4,3}(1)-N_{3,3}(1)N_{4,4}(1)\right]=0\end{aligned}\tag{76}$$

Solving the determinant yields the eigenvalues $\delta$, which enable the determination of the vibration periods.

### 4.2 Special base constraints

#### 4.2.1 Fully fixed: $\beta_R^2 \to 0, \beta_T^2 \to 0$

In this scenario, the lateral and rotational stiffnesses at the base approach infinity ($K_T \to \infty$, $K_R \to \infty$) preventing base displacements—a typical condition for conventional buildings. The characteristic equation for calculating the eigenvalue $\gamma$ is:

$$N_{3,4}(1)N_{4,3}(1)-N_{3,3}(1)N_{4,4}(1)=0\tag{77}$$

i.e.,

$$\begin{aligned}&(\xi\sinh\xi+\beta\sin\beta)\left[-\xi\left(\xi^2-\alpha^2\right)\sinh\xi+\beta\left(\beta^2+\alpha^2\right)\sin\beta\right]\\&+\left(\xi^2\cosh\xi+\beta^2\cos\beta\right)\left[\left(\xi^2-\alpha^2\right)\cosh\xi+\left(\beta^2+\alpha^2\right)\cos\beta\right]=0\end{aligned}\tag{78}$$

**4.2.2 Rotationally flexible and translationally fixed: $\beta_R^2 \neq 0, \beta_T^2 \to 0$**

In this case, only the lateral stiffness at the base tends to infinity ($K_T \to \infty$), preventing translational displacement at the base. The characteristic equation for determining the eigenvalue $\delta$ is:

$$\left[N_{3,4}(1)N_{4,2}(1)-N_{3,2}(1)N_{4,4}(1)\right]\beta_R^2+\left[N_{3,4}(1)N_{4,3}(1)-N_{3,3}(1)N_{4,4}(1)\right]=0 \tag{79}$$

i.e.,

$$\begin{aligned}&\Big[-(\xi\sinh\xi+\beta\sin\beta)\Big(-\left(\xi^2+\gamma^2\mu^2\right)\left(\xi^2-\alpha^2\right)\cosh\xi+\left(\beta^2-\gamma^2\mu^2\right)\left(\beta^2+\alpha^2\right)\cos\beta\Big)\\&+\Big(\left(\xi^2+\gamma^2\mu^2\right)\xi\sinh\xi-\left(\beta^2-\gamma^2\mu^2\right)\beta\sin\beta\Big)\Big(\left(\xi^2-\alpha^2\right)\cosh\xi+\left(\beta^2+\alpha^2\right)\cos\beta\Big)\Big]\beta_R^2\\&+\begin{bmatrix}-(\xi\sinh\xi+\beta\sin\beta)\Big(-\xi\left(\xi^2-\alpha^2\right)\sinh\xi+\beta\left(\beta^2+\alpha^2\right)\sin\beta\Big)\\+\left(\xi^2\cosh\xi+\beta^2\cos\beta\right)\Big(\left(\xi^2-\alpha^2\right)\cosh\xi+\left(\beta^2+\alpha^2\right)\cos\beta\Big)\end{bmatrix}=0\end{aligned} \tag{80}$$

**4.2.3 Rotationally free and translationally fixed: $\beta_R^2 \to \infty, \beta_T^2 \to 0$**

This case corresponds to a pinned base condition where $K_R \to 0$ and $K_T \to \infty$. The characteristic equation for determining the eigenvalue $\delta$ is:

$$N_{3,4}(1)N_{4,2}(1)-N_{3,2}(1)N_{4,4}(1)=0 \tag{81}$$

i.e.,

$$\begin{aligned}&(\xi\sinh\xi+\beta\sin\beta)\Big[-\left(\xi^2+\gamma^2\mu^2\right)\left(\xi^2-\alpha^2\right)\cosh\xi+\left(\beta^2-\gamma^2\mu^2\right)\left(\beta^2+\alpha^2\right)\cos\beta\Big]\\&+\Big[\left(\xi^2+\gamma^2\mu^2\right)\xi\sinh\xi-\left(\beta^2-\gamma^2\mu^2\right)\beta\sin\beta\Big]\Big[\left(\xi^2-\alpha^2\right)\cosh\xi+\left(\beta^2+\alpha^2\right)\cos\beta\Big]=0\end{aligned} \tag{82}$$

**4.2.4 Rotationally fixed and translationally free: $\beta_R^2 \to 0, \beta_T^2 \to \infty$**

A notable special case is that of isolated-base buildings where $K_R \to \infty$, $K_T \to 0$. In this condition, lateral displacement is permitted while rotational displacement is fully restrained. The characteristic equation for calculating the eigenvalue $\delta$ is:

$$N_{3,1}(1)N_{4,3}(1)-N_{3,3}(1)N_{4,1}(1)=0 \tag{83}$$

i.e.,

$$\begin{aligned}&\Big[\Big(\xi^2-\left(\alpha^2-\gamma^2\mu^2\right)\Big)\xi^2\cosh\xi-\Big(\beta^2+\left(\alpha^2-\gamma^2\mu^2\right)\Big)\beta^2\cos\beta\Big]\Big[-\xi\left(\xi^2-\alpha^2\right)\sinh\xi+\beta\left(\beta^2+\alpha^2\right)\sin\beta\Big]\\&+\left(\xi^2\cosh\xi+\beta^2\cos\beta\right)\Big[\Big(\xi^2-\left(\alpha^2-\gamma^2\mu^2\right)\Big)\xi\left(\xi^2-\alpha^2\right)\sinh\xi+\Big(\beta^2+\left(\alpha^2-\gamma^2\mu^2\right)\Big)\beta\left(\beta^2+\alpha^2\right)\sin\beta\Big]=0\end{aligned} \tag{84}$$

The boundary conditions considered in Sections 4.2.3 and 4.2.4, despite leading to configurations that resemble inverted-pendulum mechanisms, are included because they represent fundamental limiting cases within the full range of base stiffness conditions. Releasing either rotation or translation at the base introduces additional global degrees of freedom and shifts the deformation mechanism from bending-dominated to rotation-dominated behavior. These extreme scenarios are not intended to model common building configurations, but rather to complete the analytical characterization of the proposed formulation, to illustrate its behavior in boundary-condition limits, and to provide insight into situations relevant for highly flexible foundations, base-isolation systems, or structures with significant soil–structure interaction.

### 4.3 Modal properties

#### 4.3.1 Orthogonality of vibration modes

To prove the orthogonality of the modes, the differential equation is considered for a generic vibration mode *r*. The Eq. (55) is multiplied by $\phi_s(z)$ and integrated over the normalized height of the continuous model.

$$\int_0^1 \left[\phi_r'''' (z)\phi_s(z) - \alpha^2 \phi_r''(z)\phi_s(z)\right] dz = \gamma_r^2 \int_0^1 \left[-\mu^2 \phi_r''(z)\phi_s(z) + \phi_r(z)\phi_s(z)\right] dz \tag{85}$$

Integrating by parts and applying the boundary conditions yields:

$$\int_0^1 \left[-\phi_r''(z)\phi_s''(z) + \alpha^2 \phi_r'(z)\phi_s'(z)\right] dz = \gamma_r^2 \int_0^1 \left[\mu^2 \phi_r'(z)\phi_s'(z) + \phi_r(z)\phi_s(z)\right] dz \tag{86}$$

Similarly, considering another generic vibration mode *s*, Eq. (55) is multiplied by $\phi_r(z)$ and integrated over the beam height.

$$\int_0^1 \left[-\phi_r''(z)\phi_s''(z) + \alpha^2 \phi_r'(z)\phi_s'(z)\right] dz = \gamma_s^2 \int_0^1 \left[\mu^2 \phi_r'(z)\phi_s'(z) + \phi_r(z)\phi_s(z)\right] dz \tag{87}$$

Substituting the boundary conditions and performing subtraction yields the expression demonstrating the orthogonality of the vibration modes:

$$\left(\gamma_r^2 - \gamma_s^2\right) \int_0^1 \left[\mu^2 \phi_r'(z)\phi_s'(z) + \phi_r(z)\phi_s(z)\right] dz = 0 \tag{88}$$

#### 4.3.2 Modal analysis of forced dynamic response to ground motion

Displacements in each mode are expressed in terms of generalized coordinates as follows:

$$u(z,t) = \sum_{r=1}^{\infty} \phi_r(z) q(t) \tag{89}$$

Thus, the response of the eigenvectors is expressed as a superposition of individual vibration modes. The coupled differential equation for the *r*-th mode is rewritten as:

$$\sum_{r=1}^{\infty} \gamma_u \left[\phi_r(z) - \mu^2 \phi_r''(z)\right] \ddot{q}(t) + \sum_{r=1}^{\infty} \omega_r^2 \gamma_u \left[\phi_r(z) - \mu^2 \phi_r''(z)\right] q(t) = f(z,t) \tag{90}$$

Multiplying Eq. (90) by $\phi_s(z)$ and integrating over the beam height yields:

$$\sum_{r=1}^{\infty} \gamma_u \left[\phi_r(z)\phi_s(z) + \mu^2 \phi_r'(z)\phi_s'(z)\right] \ddot{q}(t) + \sum_{r=1}^{\infty} \omega_r^2 \gamma_u \left[\phi_r(z)\phi_s(z) + \mu^2 \phi_r'(z)\phi_s'(z)\right] q(t) = \int_0^1 f(z,t)\phi_s(z) dz \tag{91}$$

Due to the orthogonality of the mode shapes, the off-diagonal terms for $r \neq s$ vanish. Considering the diagonal terms corresponding to $r = s$, the following expression is obtained:

$$\left(\int_0^1 \gamma_u \left[\phi^2(z) + \mu^2 \phi'^2(z)\right] dz\right) \ddot{q}(t) + \left(\int_0^1 \omega^2 \gamma_u \left[\phi^2(z) + \mu^2 \phi'^2(z)\right] dz\right) q(t) = \int_0^1 f(z,t)\phi(z) dz \tag{92}$$

Reorganizing terms yields the standard single-degree-of-freedom (SDOF) equation in the form:

$$\ddot{q}(t) + \omega^2 q(t) = \frac{\int_0^1 f(z,t)\phi(z) dz}{\int_0^1 \gamma_u \left[\phi^2(z) + \mu^2 \phi'^2(z)\right] dz} \tag{93}$$

For seismic excitation, the external force term is replaced by the effective inertia force: $f(z,t) = -\gamma_u \ddot{u}_g(t)$. Then Eq. (93) becomes:

$$\ddot{q}(t) + \omega^2 q(t) = -\frac{\int_0^1 \gamma_u \phi(z) dz}{\int_0^1 \gamma_u \left[\phi^2(z) + \mu^2 \phi'^2(z)\right] dz} \ddot{u}_g(t) \tag{94}$$

i.e.,

$$\ddot{q}(t)+\omega^2 q(t)=-\Gamma\ddot{u}_g(t) \tag{95}$$

The modal parameters are defined as follows:

- Modal earthquake excitation factor:

$$L=\int_0^1 \gamma_u \phi(z)\,dz \tag{96}$$

- Generalized modal mass:

$$M=\int_0^1 \gamma_u\left[\phi^2(z)+\mu^2\phi'^2(z)\right]dz \tag{97}$$

- Modal participation factor:

$$\Gamma=\frac{\int_0^1 \gamma_u \phi(z)\,dz}{\int_0^1 \gamma_u\left[\phi^2(z)+\mu^2\phi'^2(z)\right]dz} \tag{98}$$

Assuming $q(t)=\Gamma D(t)$, the dynamic equation reduces to:

$$\ddot{D}(t)+\omega^2 D(t)=-\ddot{u}_g(t) \tag{99}$$

This corresponds to the motion equation of an equivalent SDOF system subjected to ground acceleration $\ddot{u}_g(t)$.

#### 4.3.3 Effective modal mass

The normalized effective modal mass is defined by:

$$\bar{M}_n^*=\frac{\Gamma L}{\gamma_u}=\frac{\left[\int_0^1 \phi(z)\,dz\right]^2}{\int_0^1\left[\phi^2(z)+\mu^2\phi'^2(z)\right]dz} \tag{100}$$

#### 4.3.4 Displacements

The displacement $D(t)$ is related to the pseudo-acceleration $A(t)$ by:

$$A(t)=\omega^2 D(t)\rightarrow D(t)=\frac{\gamma_u H^4}{K_b\delta^2}A(t) \tag{101}$$

The modal displacement $u(z,t)$ is given by:

$$u(z,t)=\phi(z)q(t)=\Gamma\phi(z)D(t)=\frac{\gamma_u H^4}{K_b}\cdot\frac{\Gamma\phi(z)}{\delta^2}A(t) \tag{102}$$

The maximum absolute value of $u(z,t)$ is:

$$u_{n0}=\frac{\gamma_u H^4}{K_b}\cdot\frac{\Gamma\phi(z)}{\delta^2}gS_a(T) \tag{103}$$

where $S_a(T)$ is the elastic pseudo-spectral acceleration for an SDOF oscillator with period $T$.

The corresponding normalized expression is:

$$\bar{u}_{n0}=\frac{K_b}{g\gamma_u H^4}u_{n0}=\frac{\Gamma\phi(z)}{\delta^2}S_a(T) \tag{104}$$

Additionally, the term $\Gamma\phi(z)$ can be rewritten as:

$$\Gamma\phi(z)=\frac{\int_0^1 \phi(z)\,dz}{\int_0^1\left[\phi^2(z)+\mu^2\phi'^2(z)\right]dz} \tag{105}$$

#### 4.3.5 Story drift ratios

The maximum value of the drift is obtained as:

$$u'_{n0}=\frac{\gamma_u H^4}{K_b}\cdot\frac{\Gamma\phi'(z)}{\gamma^2}gS_a(T) \tag{106}$$

The normalized form becomes:

$$\bar{u}'_{n0}=\frac{K_b}{g\gamma_u H^4}u'_{n0}=\frac{\Gamma\phi'(z)}{\delta^2}S_a(T) \tag{107}$$

#### 4.3.6 Overturning moments

The modal contribution to the overturning moment is expressed as:

$$M(z,t)=\frac{K_b}{H^2}u''(z,t)=\frac{K_b}{H^2}\Gamma\phi''(z)D(t) \tag{108}$$

or

$$M(z,t)=\frac{\gamma_u}{\gamma^2}\phi''(z,t)\Gamma A(t) \tag{109}$$

The maximum value is:

$$M_{n0}=\frac{\gamma_u}{\gamma^2}\phi''(z)\Gamma gS_a(T) \tag{110}$$

normalized as:

$$\bar{M}_{n0}=\frac{1}{g\gamma_u}M_{n0}=\frac{\Gamma\phi''(z)}{\gamma^2}S_a(T) \tag{111}$$

#### 4.3.7 Shear forces

The modal shear force is given by:

$$V(z,t)=\frac{K_b}{H^3}\left[u'''(z)-\alpha^2 u'(z)\right] \tag{112}$$

Substituting modal displacements leads to:

$$V(z,t)=\frac{K_b}{H^3}\left[\phi'''(z)-\alpha^2\phi'(z)\right]\Gamma D(t) \tag{113}$$

or

$$V(z,t)=\frac{\gamma_u H}{\gamma^2}\left[\phi'''(z)-\alpha^2\phi'(z)\right]\Gamma A(t) \tag{114}$$

The maximum shear force is:

$$V_{n0}=\frac{\gamma_u H}{\gamma^2}\left[\phi'''(z)-\alpha^2\phi'(z)\right]\Gamma g S_a(T) \tag{115}$$

normalized as:

$$\bar{V}_{n0}=\frac{1}{g\gamma_u H}V_{n0}=\frac{\Gamma\left[\phi'''(z)-\alpha^2\phi'(z)\right]}{\gamma^2}S_a(T) \tag{116}$$

## 5 Numerical investigations

### 5.1 Verification and validation for the fixed-base case

To verify the proposed analytical framework, its results are benchmarked against those obtained from Miranda's [9] parallel coupling model for bending and shear beams. The reference model adopted for comparison assumes a fixed-base condition and neglects rotational inertia. The validation is then followed by a parametric investigation of soil–structure interaction effects under four boundary conditions: fixed ($K_T \to \infty$, $K_R \to \infty$), pinned ($K_T \to \infty$, $K_R \to 0$), isolated ($K_T \to 0$, $K_R \to \infty$), and free ($K_T \to 0$, $K_R \to 0$).

#### 5.1.1 Static analysis

To evaluate the accuracy of the proposed solution for static analysis, Figs. 2–7 present the lateral displacement and interstory drift profiles for four distinct lateral load distributions governed by the dimensionless parameter $a$ [9]:

$$f(z)=W_{\max}\frac{1-e^{-az}}{1-e^{-a}} \tag{117}$$

where $W_{\max}$ denotes the peak intensity of the distributed load at the top, and $a$ is a dimensionless parameter governing the shape of the lateral load distribution [9].

The analysis considers three structural systems characterized by $\alpha$ = 0.3, indicative of a bending-dominated response; $\alpha$ = 3, representing an intermediate coupling between bending and shear effects; and $\alpha$ = 15, corresponding to a shear-dominated behavior. Notably, the proposed model exhibits excellent agreement with the reference solution developed by Miranda [9].

For simplicity, Figs. 2–4 use the normalized displacement $\tilde{u}(z)$ and $\tilde{u}'(z)$, defined as:

$$\tilde{u}(z)=u(z)\frac{W_{\max}K_b}{H^4} \tag{118}$$

$$\tilde{u}'(z)=u'(z)\frac{W_{\max}K_b}{H^3} \tag{119}$$

The lateral displacement and interstory drift profiles are presented for the fixed-base condition (Fig. 5), pinned-base condition (Fig. 6), isolated-base condition (Fig. 7), and free-base condition (Fig. 8), thereby capturing the influence of soil flexibility on the structural response.

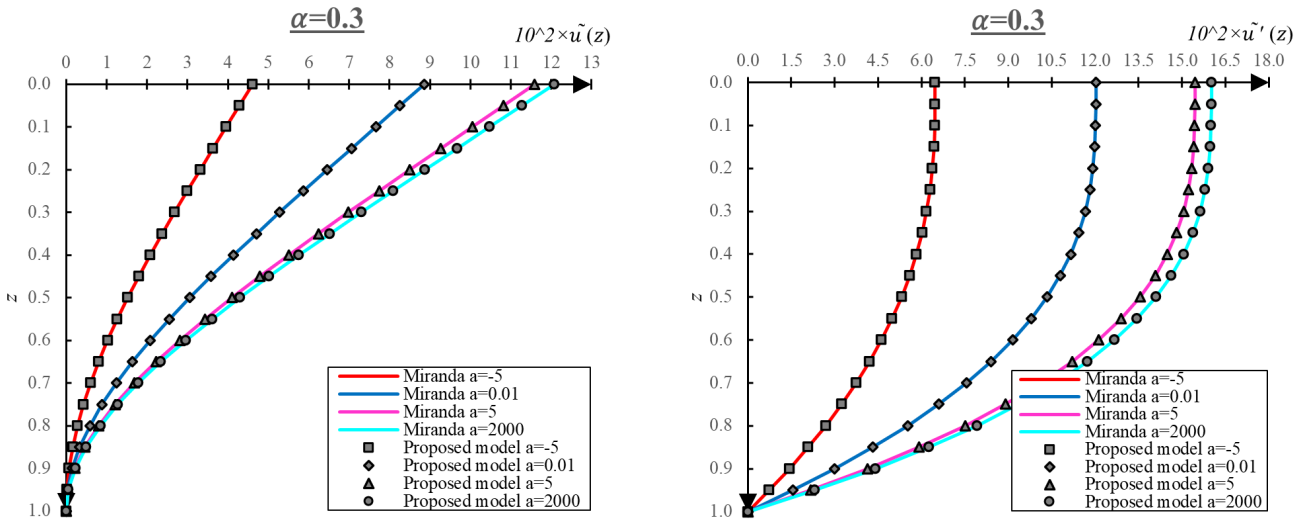


**Fig. 2** Lateral displacement and Interstory drift profiles for $\alpha$ = 0.3, representing a bending-dominated structural response

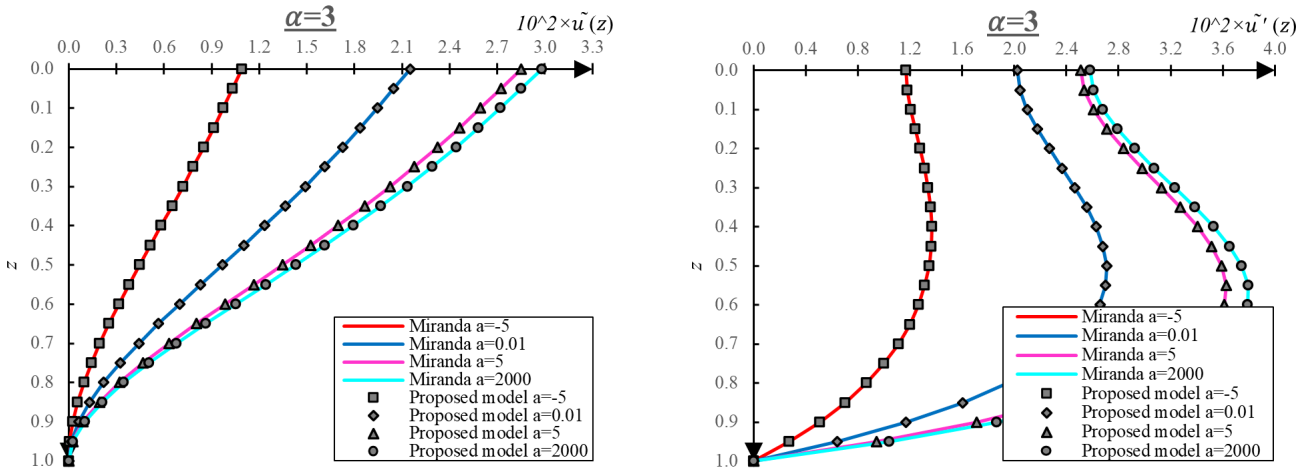


**Fig. 3** Lateral displacement and Interstory drift profiles for $\alpha = 3$, representing intermediate coupling between bending and shear behavior

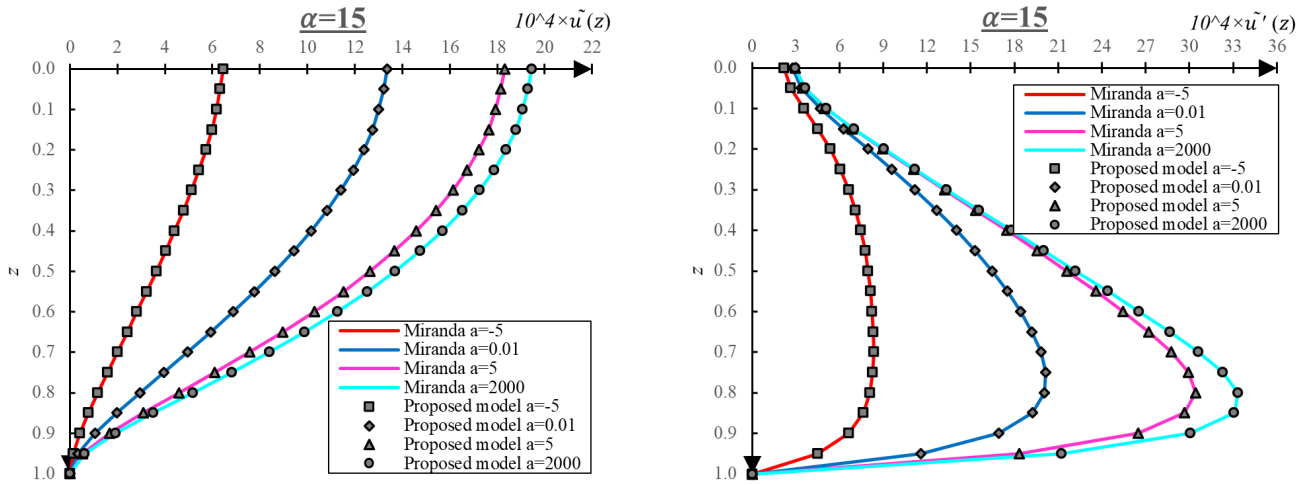


**Fig. 4** Lateral displacement and Interstory drift profiles for $\alpha = 15$, representing a shear-dominated structural response

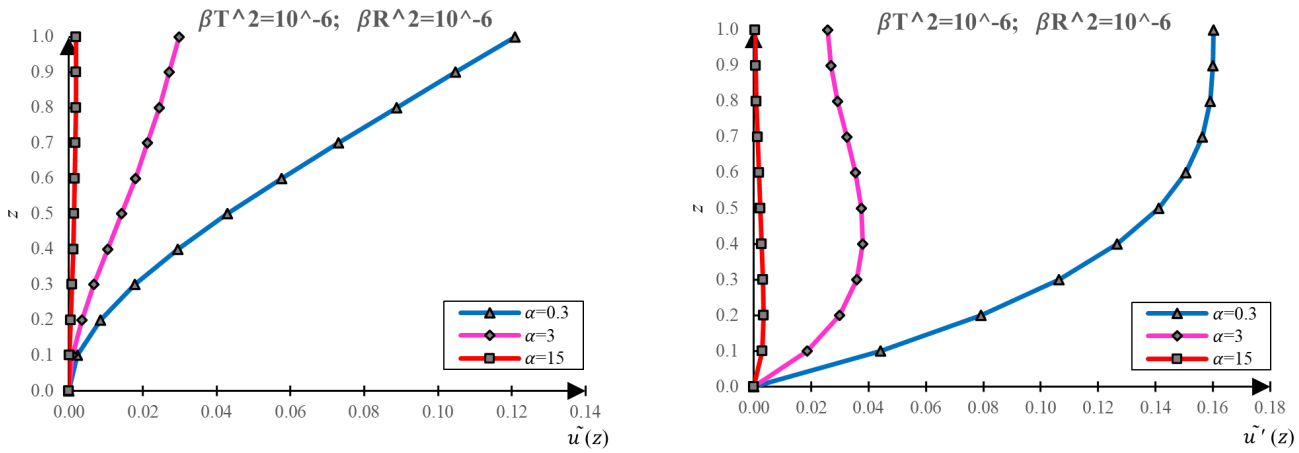


**Fig. 5** Fixed-base condition: Lateral displacement and Interstory drift profiles for $\alpha = 0.3$, $\alpha = 3$ and $\alpha = 15$

In Figs. 7 and 8, the extremely large abscissa values (on the order of $10^6$) correspond to the limiting case of vanishing translational stiffness at the base. Because the horizontal axis is expressed in terms of compliance—or, equivalently, in a normalized form involving the inverse of the translational spring stiffness—the corresponding values become very large as the base stiffness approaches zero. This behavior does not imply infinite translation of the building;

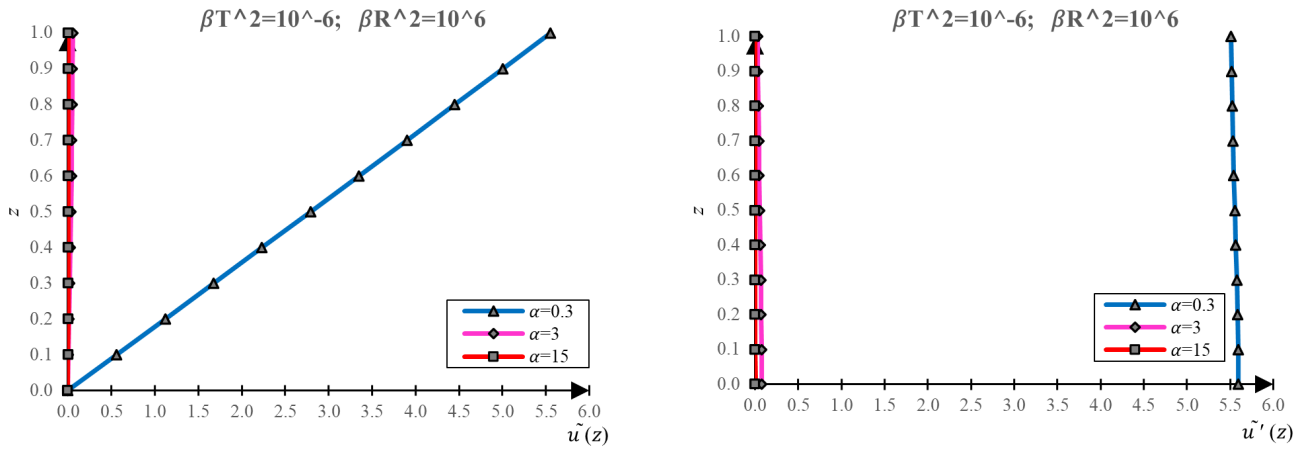


**Fig. 6** Pinned-base condition: Lateral displacement and Interstory drift profiles for $\alpha = 0.3$, $\alpha = 3$ and $\alpha = 15$

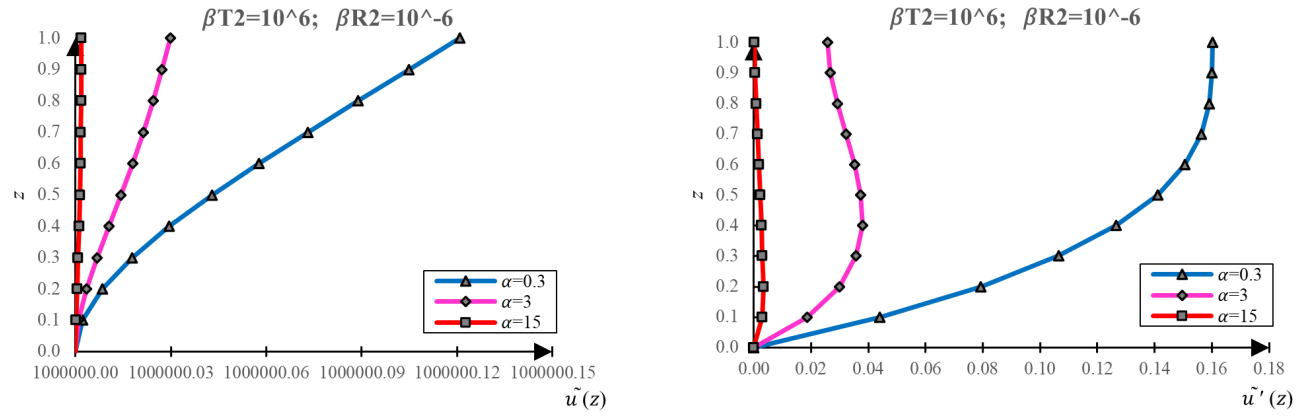


**Fig. 7** Isolated-base condition: Lateral displacement and Interstory drift profiles for $\alpha = 0.3$, $\alpha = 3$ and $\alpha = 15$

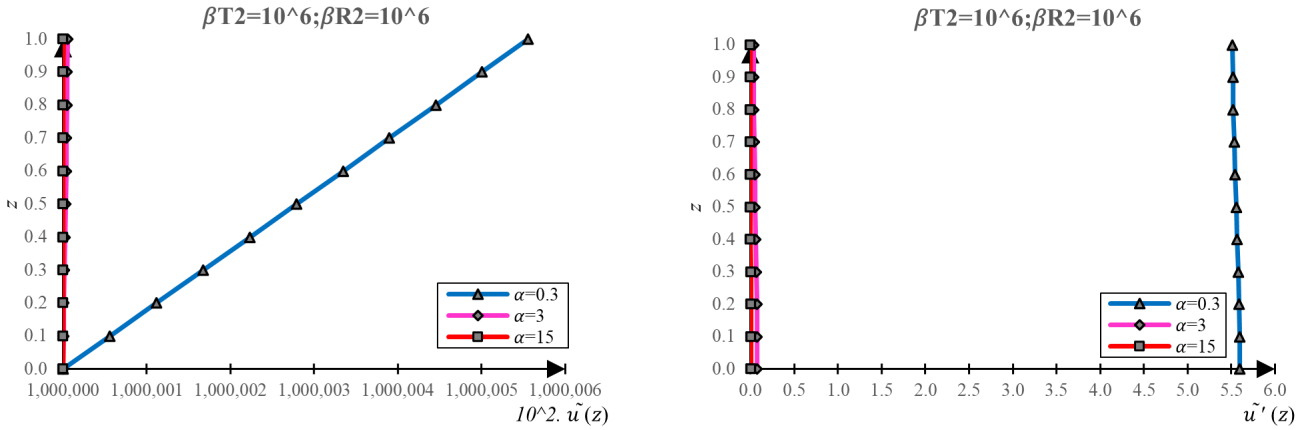


**Fig. 8** Free-base condition: Lateral displacement and Interstory drift profiles for $\alpha = 0.3$, $\alpha = 3$ and $\alpha = 15$

rather, it reflects the theoretical boundary condition of a fully free or nearly free base. These cases are included to illustrate the asymptotic behavior of the proposed formulation and to complete the parametric spectrum between perfectly fixed and fully flexible foundations.

### 5.1.2 Dynamic analysis

To evaluate the accuracy of the proposed solution for dynamic analysis, Fig. 9 presents the computed eigenvalues corresponding to the first five vibration modes while neglecting rotational inertia effects. The analysis spans

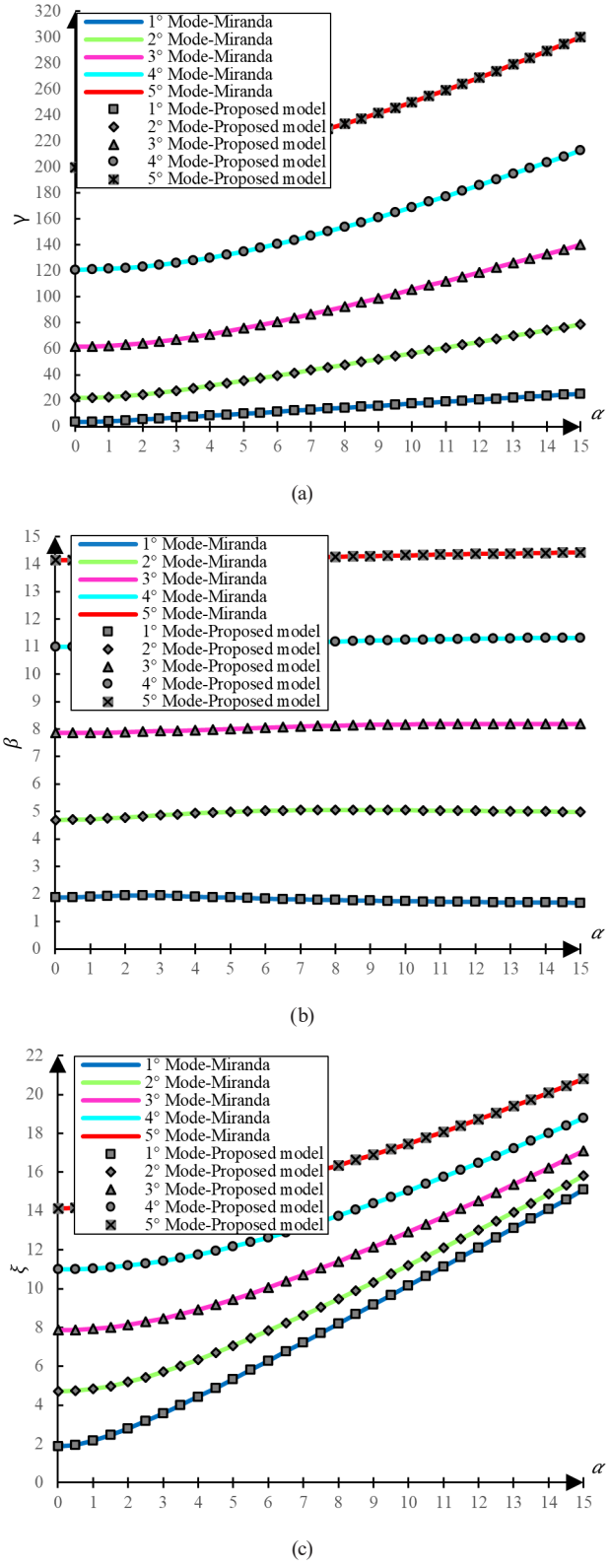


**Fig. 9** Fixed-base condition ($\mu = 0$): (a) Eigenvalue $\gamma$, (b) Eigenvalue $\beta$ and (c) Eigenvalue $\xi$ for the first five vibration modes

a broad range of structural configurations by varying the parameter $\alpha$ from 0, representing pure bending behavior, to 15, indicative of a shear-dominated response.

The results demonstrate a high degree of consistency between the proposed solution and the reference solution developed by Miranda [9], thereby confirming the accuracy of the analytical approach.

The 25-story SE Executive Tower (Fig. 10), previously analyzed by Huergo and Hernández [35], is employed as a benchmark to compare the dynamic response of a structure founded on rigid soil. The objective is to evaluate the accuracy of the proposed formulation in estimating the fundamental vibration periods. The relevant structural parameters are as follows: total height $H = 93.65$ m; distributed mass $\gamma_u = 112500$ kg/m; bending stiffnesses $K_{bx} = 2.0637 \times 10^9$ kN m$^2$ and $K_{by} = 5.1913 \times 10^8$ kN m$^2$; and shear stiffnesses $K_{sx} = 2.1178 \times 10^6$ kN and $K_{by} = 2.5008 \times 10^6$ kN. The first three natural periods computed using the proposed model are compared with those reported in [35].

Table 1 presents the first three natural vibration periods of the SE Executive Tower in the $x$- and $y$-directions under a fixed-base condition. The results show excellent agreement between the proposed analytical solutions and those obtained from finite element simulations performed using SAP2000 [41].

Subsequently, a parametric analysis is conducted to compute the eigenvalues corresponding to the first five vibration modes by varying the parameter $\alpha$ under four boundary conditions: fixed base, pinned base, isolated base, and free base. The influence of soil flexibility is explicitly accounted for in all cases, as illustrated in Figs. 11–15.

### 5.1.3 Influence of rotational inertia on the eigenvalue $\gamma$

The classical model developed by Miranda [9] neglects rotational inertia in the dynamic formulation. To assess the implications of this assumption, the influence of explicitly incorporating rotational inertia on the first three vibration modes is examined under four boundary conditions: fixed, pinned, isolated, and free. The comparative results are presented in Figs. 16–19. The effect of rotational inertia is found to be nearly negligible for the fundamental vibration mode, which explains its widespread omission in the existing literature. However, for higher modes, its influence becomes significant and increases with both the mode number and the dimensionless parameter $\alpha$, particularly in shear-dominated configurations.

The influence of rotational inertia is generally negligible for the fundamental mode of tall buildings whose lateral response is dominated by bending and whose mass distribution varies smoothly along the height. However,

(a)

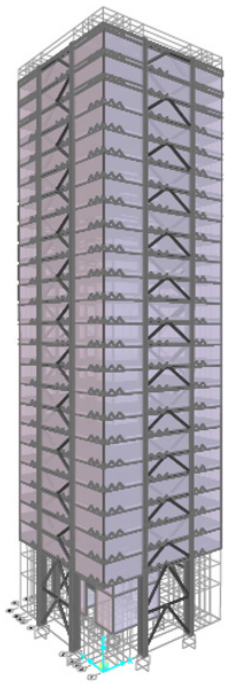

(b)

**Fig. 10** SE Executive Tower with fixed-base support: (a) General view of the building and (b) Finite element model (FEM) representation

**Table 1** First three periods of the SE Executive Tower with fixed-base support

| Mode | *X*-direction | | | *Y*-direction | | |
|---|---|---|---|---|---|---|
| | FEM (s) | CM (s) | Error | FEM (s) | CM (s) | Error |
| 1 | 1.871 | 1.859 | −0.66% | 2.089 | 2.095 | 0.32% |
| 2 | 0.470 | 0.464 | −1.19% | 0.617 | 0.62 | 0.54% |
| 3 | 0.194 | 0.192 | −1.22% | 0.301 | 0.308 | 2.30% |

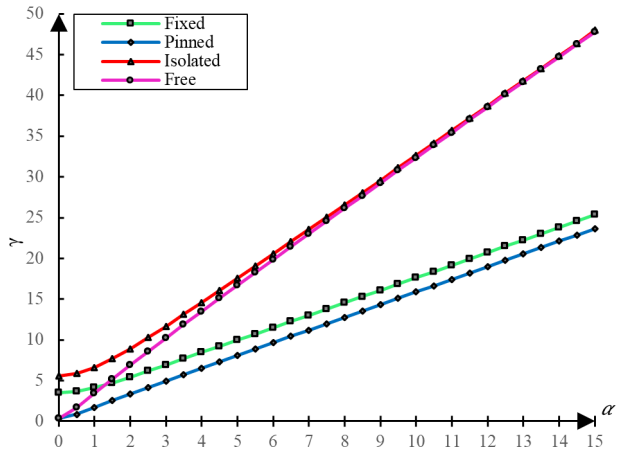


(a)

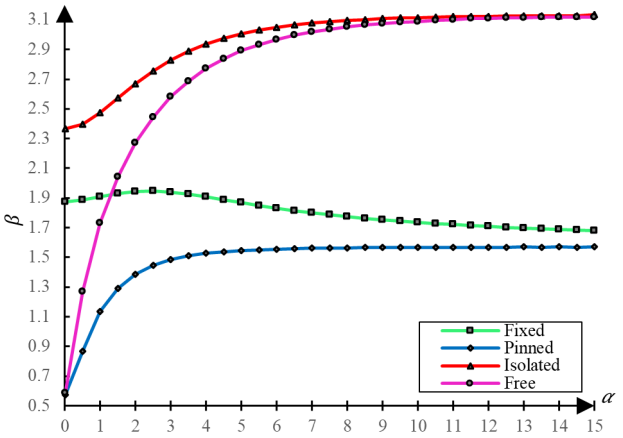


(b)

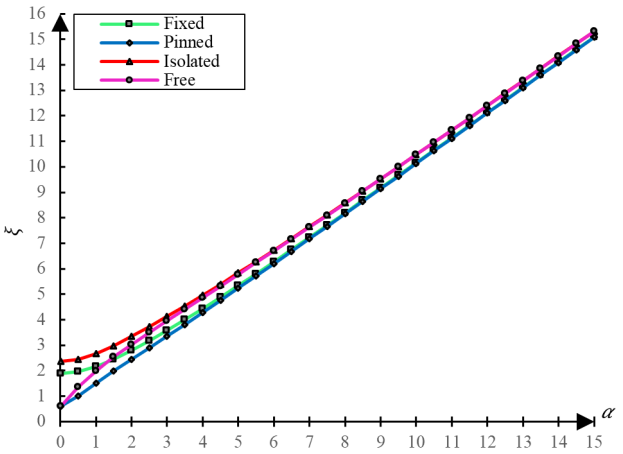


(c)

**Fig. 11** First vibration mode for $\mu = 0$: (a) Eigenvalue $\gamma$, (b) Eigenvalue $\beta$ and (c) Eigenvalue $\xi$ under varying base conditions

its contribution becomes significant in several practical situations, including structures dominated by shear deformation, such as buildings with slender structural walls or closely spaced coupling beams; systems with relatively low bending stiffness compared with shear stiffness, in which higher modes exhibit increased curvature concentration;

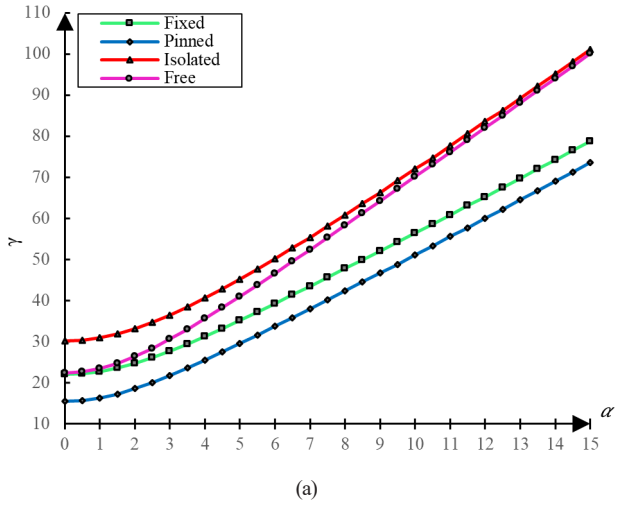


(a)

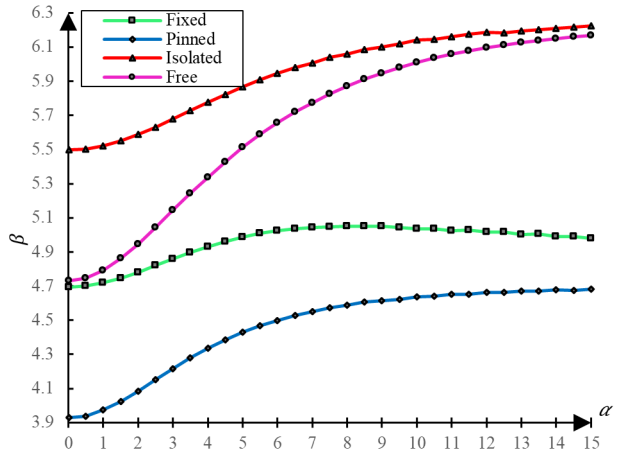


(b)

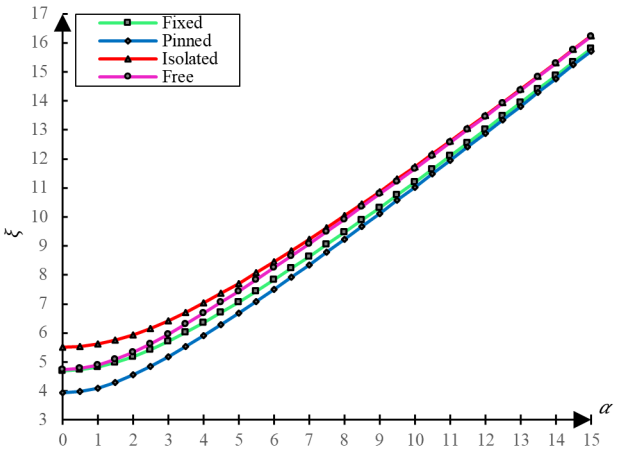


(c)

**Fig. 12** Second vibration mode for $\mu = 0$: (a) Eigenvalue $\gamma$, (b) Eigenvalue $\beta$ and (c) Eigenvalue $\xi$ under varying base conditions

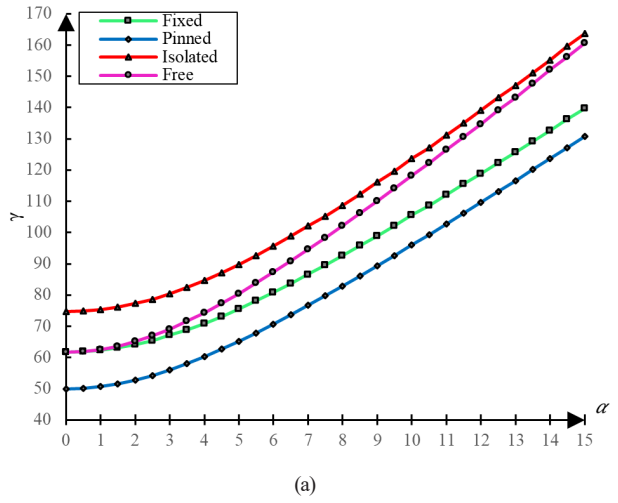


(a)

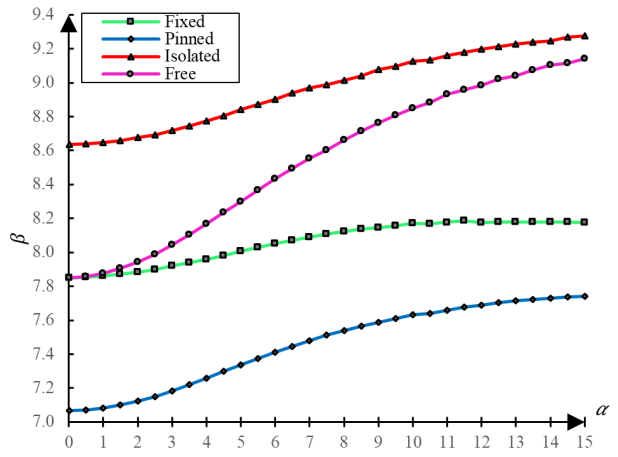


(b)

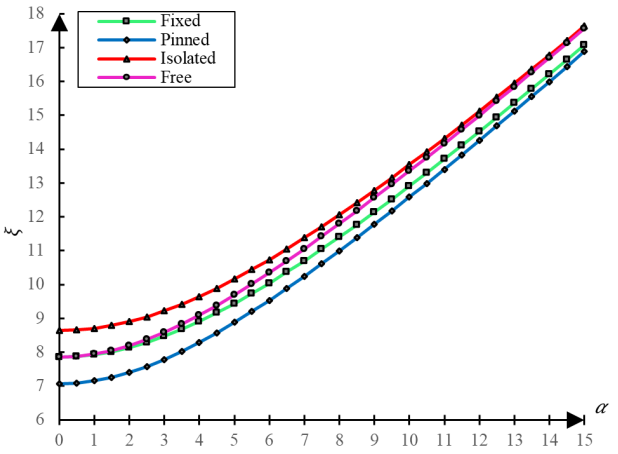


(c)

**Fig. 13** Third vibration mode for $\mu = 0$: (a) Eigenvalue $\gamma$, (b) Eigenvalue $\beta$ and (c) Eigenvalue $\xi$ under varying base conditions

buildings supported on flexible foundations, base-isolated systems, or soil–structure interaction conditions that amplify the contribution of higher vibration modes; and configurations in which the upper modes develop substantial rotation gradients. In such cases, neglecting rotational inertia may lead to an underestimation of higher-mode frequencies and an inaccurate representation of mode shapes. The proposed formulation overcomes these limitations by explicitly incorporating rotational inertia in both the static and dynamic analyses.

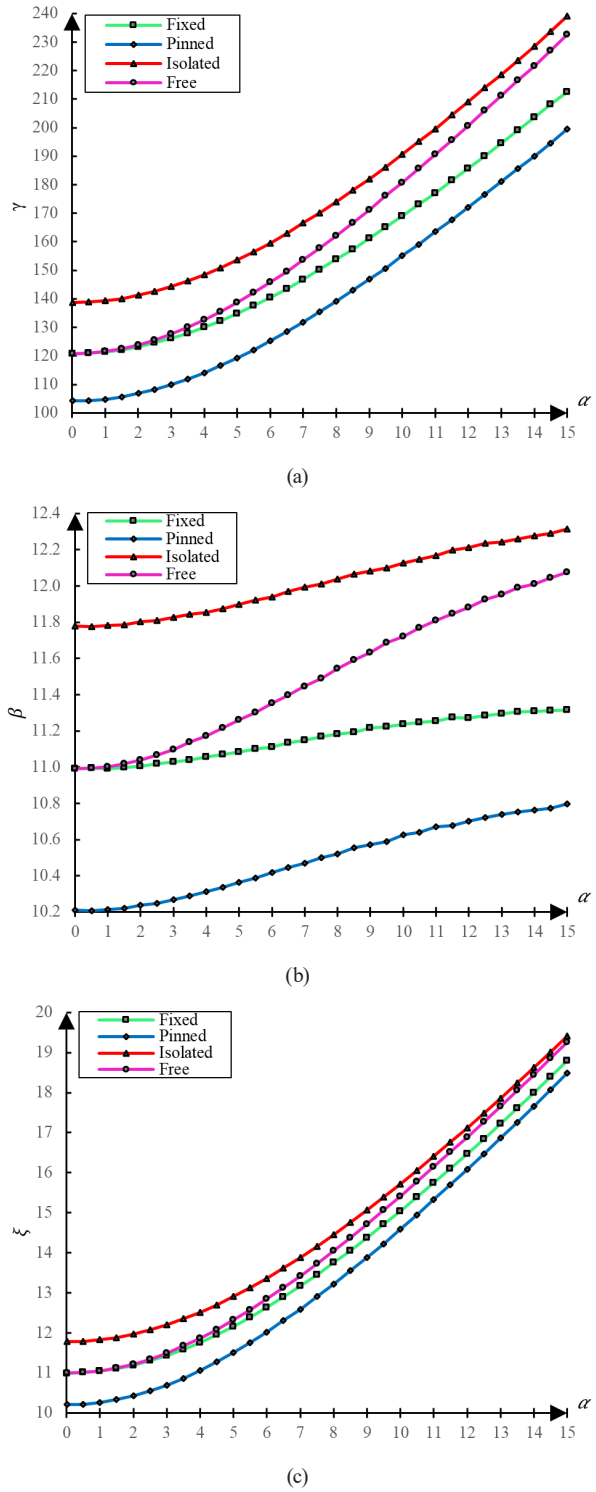


**Fig. 14** Fourth vibration mode for $\mu = 0$: (a) Eigenvalue $\gamma$, (b) Eigenvalue $\beta$ and (c) Eigenvalue $\xi$ under varying base conditions

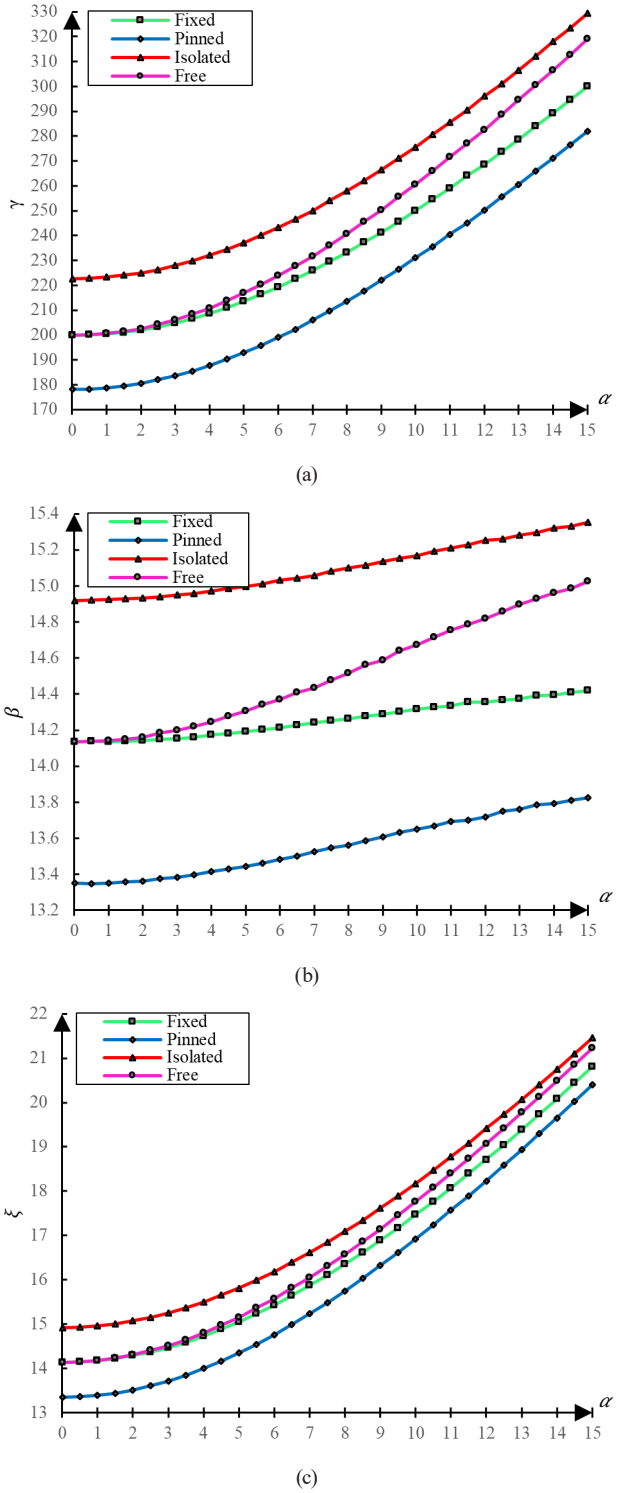


**Fig. 15** Fifth vibration mode for $\mu = 0$: (a) Eigenvalue $\gamma$, (b) Eigenvalue $\beta$ and (c) Eigenvalue $\xi$ under varying base conditions

### 5.1.4 Parametric analysis considering soil flexibility

To validate the applicability of the proposed solution in the limiting cases of bending- and shear-dominated behavior, the influence of soil flexibility on the eigenvalue associated with the vibration period is examined. For this purpose, a comprehensive parametric study is conducted, comprising 91 simulations for each limiting case. To encompass the full spectrum of possible soil conditions, the dimensionless parameters governing translational and rotational soil flexibility are varied over the wide ranges $\beta_T^2 = 10^{-7} - 10^7$ and $\beta_R^2 = 10^{-7} - 10^7$, thereby covering all boundary conditions from fully free to fully fixed bases.

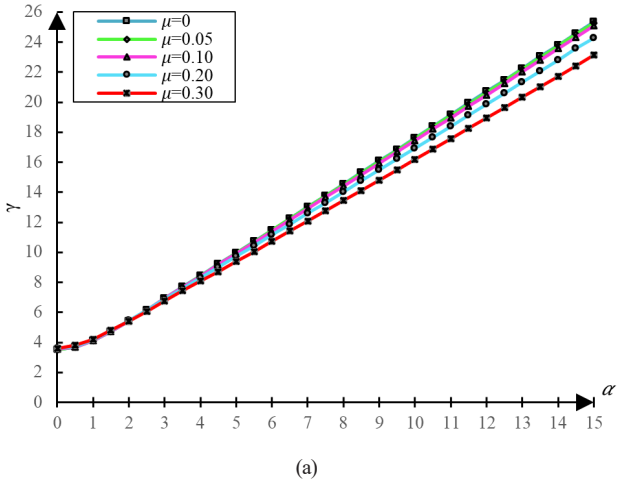


(a)

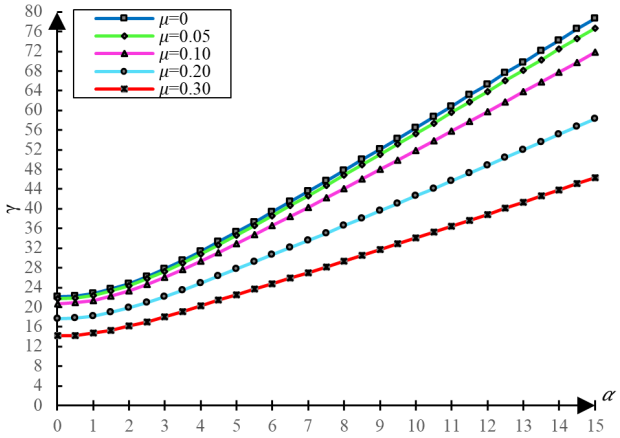


(b)

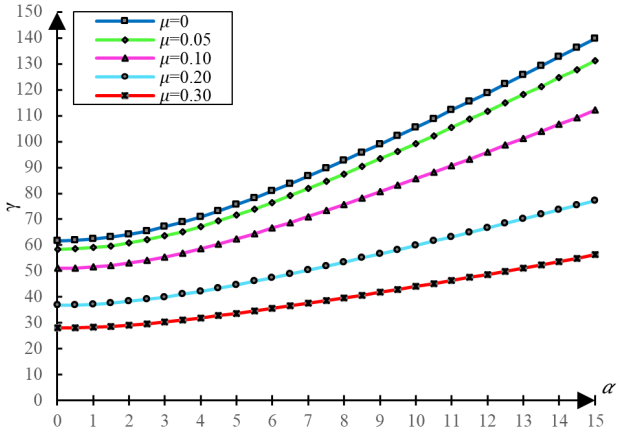


(c)

**Fig. 16** Fixed-base condition: Influence of rotational inertia ($\mu$) on the eigenvalue $\gamma$ for the first, second, and third vibration modes

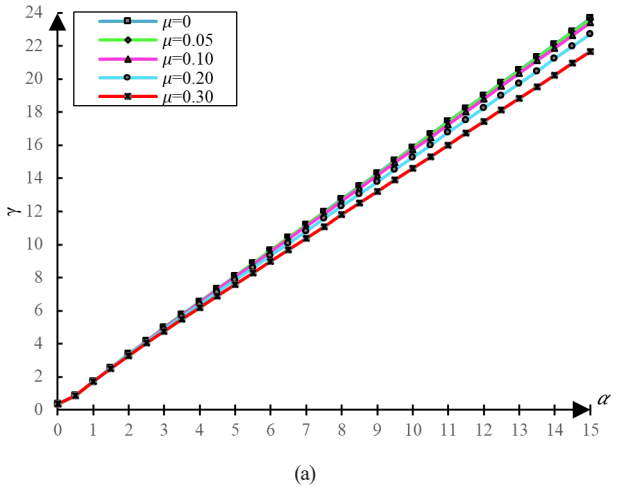


(a)

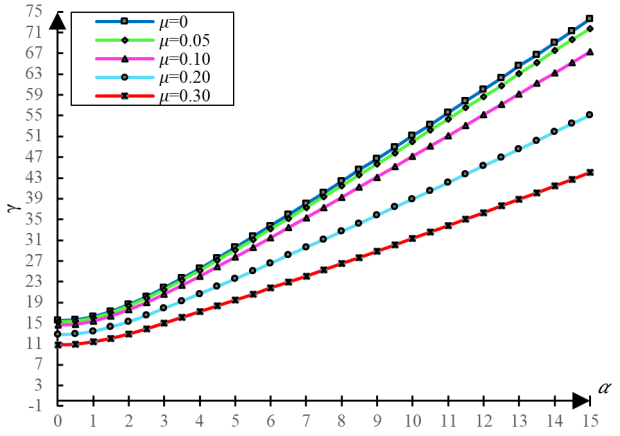


(b)

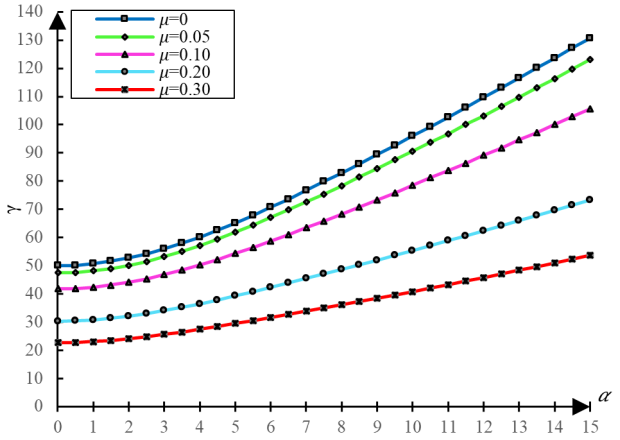


(c)

**Fig. 17** Pinned-base condition: Influence of rotational inertia ($\mu$) on the eigenvalue $\gamma$ for the first, second, and third vibration modes

Fig. 20 presents the eigenvalue results for the case $\alpha = 0$, corresponding to a purely bending response, in comparison with exact solutions obtained from a classical bending beam model. An excellent agreement is observed over the entire range of soil flexibility.

Similarly, Fig. 21 presents the eigenvalue results for the case $\alpha = 27.5$, representative of an approximately pure shear response. These results are compared with exact solutions derived from a shear-dominated beam model, revealing excellent agreement, particularly for scenarios characterized by high soil flexibility.

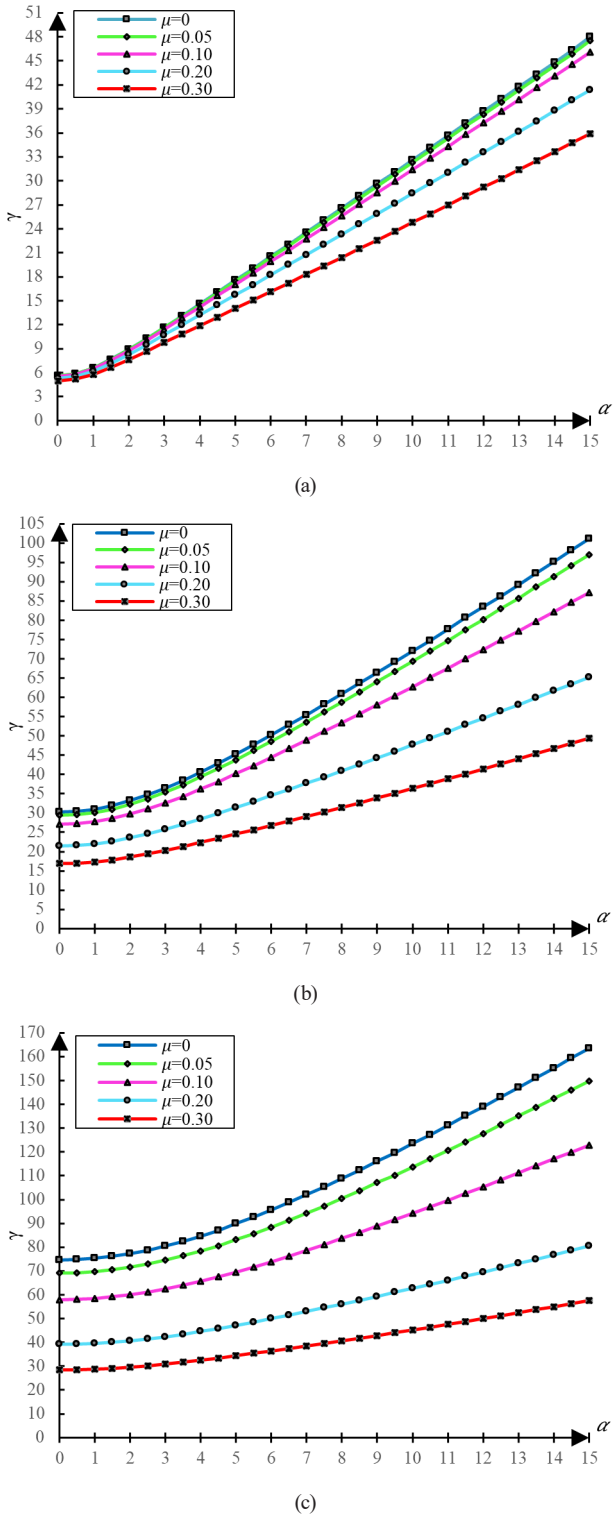


**Fig. 18** Isolated-base condition: Influence of rotational inertia ($\mu$) on the eigenvalue $\gamma$ for the first, second, and third vibration modes

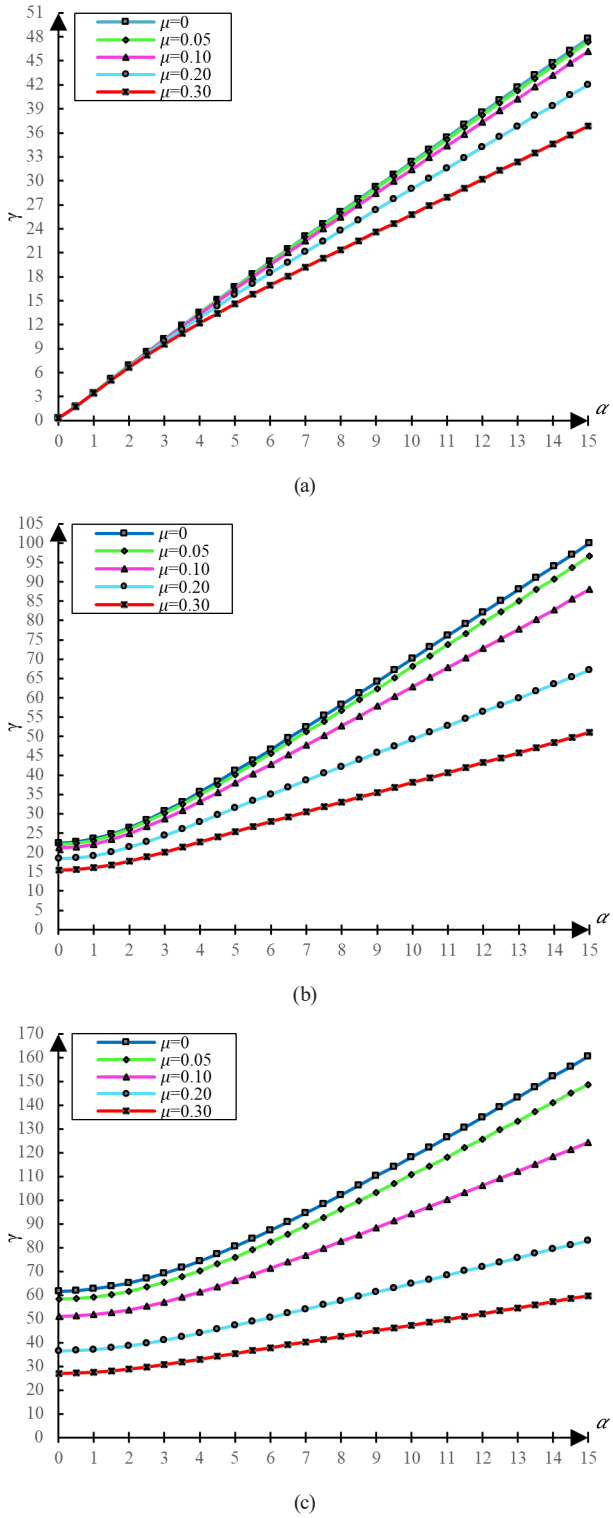


**Fig. 19** Free-base condition: Influence of rotational inertia ($\mu$) on the eigenvalue $\gamma$ for the first, second, and third vibration modes

## 6 Conclusions and future work

The main contributions and findings of this study are summarized as follows:

- A continuous analytical model for tall buildings is developed based on the parallel coupling of a bending beam and a shear beam, extending classical formulations by explicitly incorporating foundation flexibility and rotational inertia.
- The governing equations and boundary conditions are rigorously derived within a variational framework. Closed-form solutions are obtained for uniform buildings via the Laplace transform, and

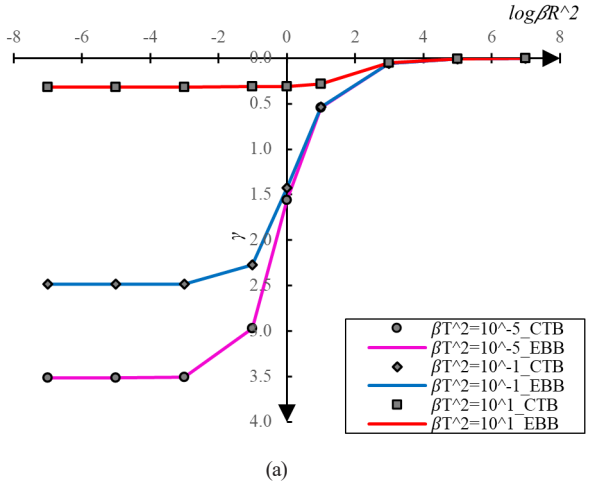


(a)

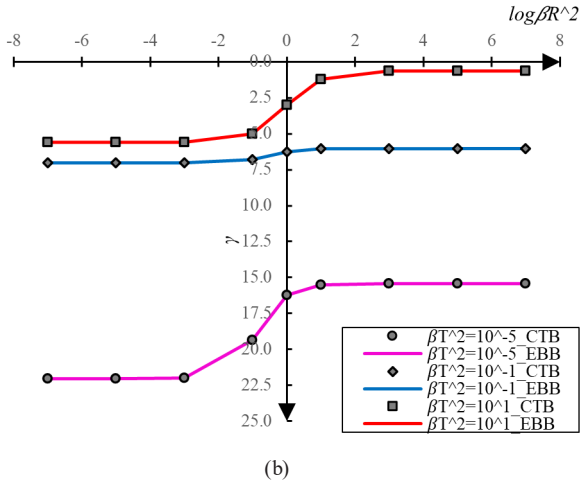


(b)

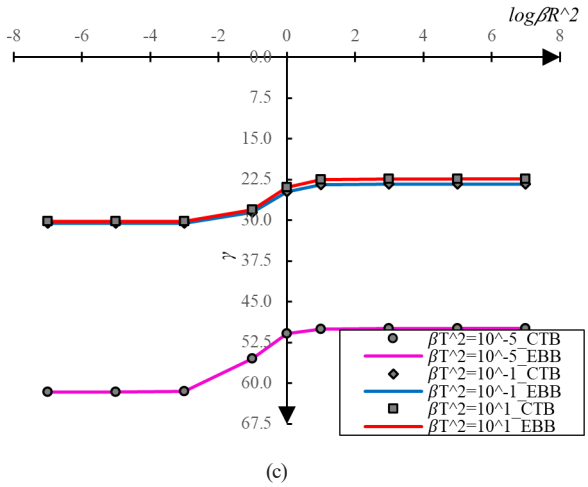


(c)

**Fig. 20** Comparison of eigenvalues for the pure bending case ($\alpha = 0$) with $\mu = 0$, corresponding to the (a) first, (b) second, and (c) third vibration modes

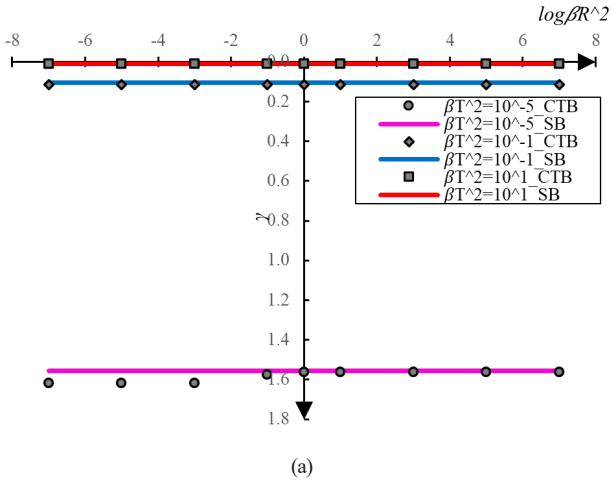


(a)

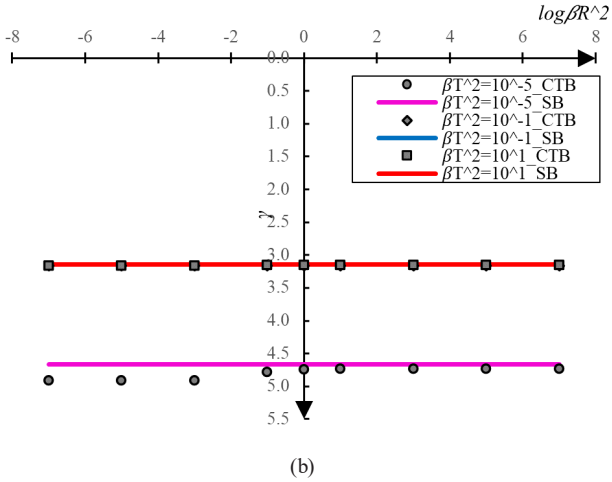


(b)

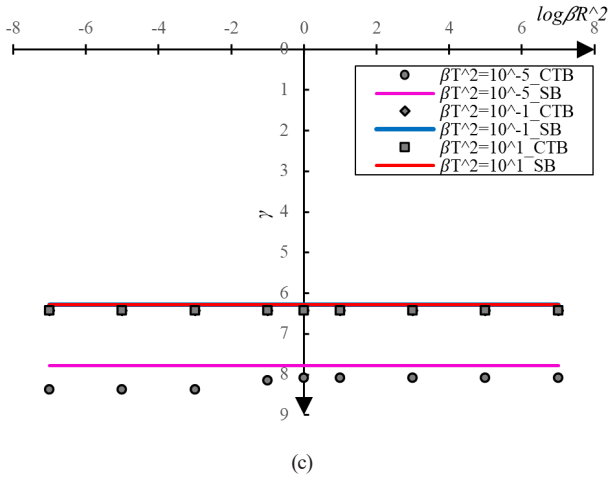


(c)

**Fig. 21** Comparison of eigenvalues for the pure shear case ($\alpha = 27.5$) with $\mu = 0$, corresponding to the (a) first, (b) second, and (c) third vibration modes

a modified transfer matrix method is introduced for non-uniform systems, avoiding matrix inversion and improving computational efficiency.

- The model captures bending-dominated, shear-dominated, and coupled responses by varying the relative magnitudes of bending and shear stiffnesses, and it accommodates arbitrary lateral load distributions.
- Rotational inertia—often neglected in previous continuous models—is shown to have a negligible influence on the fundamental mode but a significant effect

on higher modes, especially in shear-dominated configurations and under flexible-base conditions.

- Validation against Miranda's [9] fixed-base continuous bending–shear model and finite element simulations demonstrates strong agreement across bending- and shear-dominated regimes. A comprehensive parametric study covering more than 182 cases confirms the robustness and accuracy of the proposed formulation under varying soil–structure stiffness ratios.
- The model provides a practical and computationally efficient tool for preliminary design and sensitivity analyses of tall buildings, enabling the inclusion of soil–structure interaction and higher-mode effects without the computational demands of detailed finite element models.

It is important to note that the proposed model does not account for second-order ($P$–$\Delta$) effects or stiffness reductions associated with geometric instability. Consequently, its applicability is restricted to structures that remain within the linear elastic range and whose lateral displacements do not induce significant second-order amplification. Under these conditions, the formulation is suitable for tall buildings with adequate lateral stiffness and seismic acceleration levels that do not produce excessive drifts.

Future extensions of the model may include the incorporation of second-order ($P$–$\Delta$) effects and geometric-stiffness degradation; nonlinear soil–structure interaction, including hysteretic and radiation damping mechanisms; advanced damping models and energy-dissipation mechanisms; and application of the formulation to performance-based seismic design of tall buildings and systems with base isolation or highly flexible foundations.

**Acknowledgments**

The author dedicates this modest scientific contribution to his beloved daughter, Zoé Juliette Pinto Pereira. My dear child, how wonderful it is to see you grow day by day. I love you!

"*One day, posterity will laugh at the foolishness of modern materialist philosophers. The more I study nature, the more astonished I am by the work of the Creator. I pray while I am engaged in my work in the laboratory. Blessed is the one who carries within himself a God, an ideal, and obeys it—the ideal of art, the ideal of the virtues of the Gospel. These are the sources of great thoughts. All these reflections reflect the light of the infinit*" (Louis Pasteur)

"*You, young men and scientists of the future: do not allow yourselves to be contaminated by sterile skepticism, nor be discouraged by the sadness of certain hours that weigh upon nations. Do not become angry with your opponents, for no scientific theory has ever been accepted without opposition. Live in the serene peace of libraries and laboratories. Say to yourselves, first: what have I done for my education? and, as you advance step by step: what am I accomplishing? until the time comes when you can have the immense joy of thinking that you have contributed in some way to the well-being and progress of humanity.*" (Louis Pasteur)

**Conflicts of interest**

The author declares no conflicts of interest.

**Data availability statement**

The data that support the findings of this study are available from the corresponding author upon reasonable request.

**References**

[1] Jacobsen, L. S. "Motion of a Soil Subjected to a Simple Harmonic Ground Motion Vibration", Bulletin of the Seismological Society of America, 20(3), pp. 160–195, 1930. https://doi.org/10.1785/BSSA0200030160

[2] Biot, M. "Theory of Elastic Systems Vibrating under Transient Impulse with an Application to Earthquake-Proof Buildings", Proceedings of the National Academy of Sciences of the United States of America, 19(2), pp. 262–268, 1933. https://doi.org/10.1073/pnas.19.2.262

[3] Chitty, L. "LXXVIII. On the cantilever composed of a number of parallel beams interconnected by cross bars", The London, Edinburgh, and Dublin Philosophical Magazine and Journal of Science, 38(285), pp. 685–699, 1947. https://doi.org/10.1080/14786444708521646

[4] Chitty, L., Wan, W. Y. "Tall building structures under wind load", In: Proceedings of the 7th International Congress for Applied Mechanics, London, UK, 1948, pp. 254–268.

[5] Skattum, K. S. "Dynamic analysis of coupled shear walls and sandwich beams", Earthquake Engineering Research Laboratory, California Institute of Technology, Pasadena, CA, USA, Rep. EERL 71-06, 1971.

[6] Rosman, R. "Buckling and vibrations of spatial building structures", Engineering Structures, 3(4), pp. 194–202, 1981. https://doi.org/10.1016/0141-0296(81)90001-8

[7] Rosman, R. "Dynamics and stability of shear wall building structures", Proceedings of the Institution of Civil Engineers, 55(2), pp. 411–423, 1973. https://doi.org/10.1680/iicep.1973.4875

[8] Hegedűs, I., Kollár, L. P. "Buckling of sandwich columns with thick faces subjected to axial loads of arbitrary distribution", Acta Technica Academiae Scientiarum Hungaricae, 97(1–4), pp. 123–131, 1984.

[9] Miranda, E. "Approximate Seismic Lateral Deformation Demands in Multistory Buildings", Journal of Structural Engineering, 125(4), pp. 417–425, 1999. https://doi.org/10.1061/(ASCE)0733-9445(1999)125:4(417)

[10] Potzta, G., Kollár, L. P. "Analysis of building structures by replacement sandwich beams", International Journal of Solids and Structures, 40(3), pp. 535–553, 2003. https://doi.org/10.1016/S0020-7683(02)00622-4

[11] Zalka, K. A. "A simple method for the deflection analysis of tall wall-frame building structures under horizontal load", The Structural Design of Tall and Special Buildings, 18(3), pp. 291–311, 2009. https://doi.org/10.1002/tal.410

[12] Bozdogan, K. B. Ozturk, D., Nuhoglu, A. "An approximate method for static and dynamic analyses of multi-bay coupled shear walls", The Structural Design of Tall and Special Buildings, 18(1), pp. 1–12, 2009. https://doi.org/10.1002/tal.390

[13] Bozdogan, K. B., Ozturk, D. "A method for static and dynamic analyses of stiffened multi-bay coupled shear walls", Structural Engineering and Mechanics, 28(4), pp. 479–489, 2008. https://doi.org/10.12989/sem.2008.28.4.479

[14] Bozdogan, K. B. "An approximate method for static and dynamic analyses of symmetric wall-frame buildings", The Structural Design of Tall and Special Buildings, 18(3), pp. 279–290, 2009. https://doi.org/10.1002/tal.409

[15] Bozdogan, K. B. "Differential quadrature method for free vibration analysis of coupled shear walls", Structural Engineering and Mechanics, 41(1), pp. 67–81, 2012. https://doi.org/10.12989/sem.2012.41.1.067

[16] Catal, H. H. "A method for static and dynamic analyses of stiffened multi-bay coupled shear walls", Structural Engineering and Mechanics, 31(3), pp. 367–369, 2009. https://doi.org/10.12989/sem.2009.31.3.367

[17] Chesnais, C., Boutin, C., Hans, S. "Structural Dynamics and Generalized Continua", In: Altenbach, H., Maugin, G., Erofeev, V. (eds.) Mechanics of Generalized Continua, Springer, 2011, pp. 57–76. ISBN 978-3-642-19218-0 https://doi.org/10.1007/978-3-642-19219-7_3

[18] Zalka, K. A. "Maximum deflection of symmetric wall-frame buildings", Periodica Polytechnica Civil Engineering, 57(2), pp. 173–184, 2013. https://doi.org/10.3311/PPci.7172

[19] Capsoni, A., Moghadasi Faridani, H. "Novel continuum models for coupled shear wall analysis", The Structural Design of Tall and Special Buildings, 25(10), pp. 444–467, 2016. https://doi.org/10.1002/tal.1267

[20] Wang, R.-T., Hu, H.-S., Guo, Z.-X. "Analytical study of stiffened multibay planar coupled shear walls", Engineering Structures, 244, 112770, 2021. https://doi.org/10.1016/j.engstruct.2021.112770

[21] Laier, J. E. "An improved continuous medium technique for three-dimensional analysis of tall building structures", Structural Engineering and Mechanics, 80(1), pp. 73–81, 2021. https://doi.org/10.12989/sem.2021.80.1.073

[22] Franco, C., Chesnais, C., Semblat, J.-F., Giry, C., Desprez, C. "Finite element formulation of a homogenized beam for reticulated structure dynamics", Computers and Structures, 261–262, 106729, 2022. https://doi.org/10.1016/j.compstruc.2021.106729

[23] Ambrosini, R. D. "Material damping vs. radiation damping in soil–structure interaction analysis", Computers and Geotechnics, 33(2), pp. 86–92, 2006. https://doi.org/10.1016/j.compgeo.2006.03.001

[24] Nakhaei, M., Ali Ghannad, M. "The effect of soil–structure interaction on damage index of buildings", Engineering Structures, 30(6), pp. 1491–1499, 2008. https://doi.org/10.1016/j.engstruct.2007.04.009

[25] Medina, C., Aznárez, J. J., Padrón, L. A., Maeso, O. "Effects of soil–structure interaction on the dynamic properties and seismic response of piled structures", Soil Dynamics and Earthquake Engineering, 53, pp. 160–175, 2013. https://doi.org/10.1016/j.soildyn.2013.07.004

[26] Cheng, M. H., Heaton, T. H. "Simulating Building Motions Using Ratios of the Building's Natural Frequencies and a Timoshenko Beam Model", Earthquake Spectra, 31(1), pp. 403–420, 2015. https://doi.org/10.1193/011613EQS003M

[27] Shirzad-Ghaleroudkhani, N., Mahsuli, M., Ghahari, S. F., Taciroglu, E. "Bayesian identification of soil-foundation stiffness of building structures", Structural Control Health Monitoring, 25(3), e2090, 2018. https://doi.org/10.1002/stc.2090

[28] Taciroglu, E., Ghahari, S. F., Abazarsa, F. "Efficient model updating of a multi-story frame and its foundation stiffness from earthquake records using a timoshenko beam model", Soil Dynamics and Earthquake Engineering, 92, pp. 25–35, 2017. https://doi.org/10.1016/j.soildyn.2016.09.041

[29] Di, B., Fu, X. "Seismic Behavior of Shear Wall-Frame Systems Considering Foundation Stiffness", International Journal of Structural Stability and Dynamics, 17(3), 1750041, 2017. https://doi.org/10.1142/S0219455417500419

[30] Kara, D., Bozdogan, K. B., Keskin, E. „A simplified method for free vibration analysis of wall frames considering soil structure interaction", Structural Engineering and Mechanics, 77(1), pp. 37–46, 2021. https://doi.org/10.12989/sem.2021.77.1.037

[31] Ganjavi, B., Hajirasouliha, I., Bolourchi, A. "Optimum lateral load distribution for seismic design of nonlinear shear-buildings considering soil-structure interaction", Soil Dynamics and Earthquake Engineering, 88, pp. 356–368, 2016. https://doi.org/10.1016/j.soildyn.2016.07.003

[32] Ai, Z. Y., Cai, J. B. "Static interaction analysis between a Timoshenko beam and layered soils by analytical layer element/boundary element method coupling", Applied Mathematical Modelling, 40(21–22), pp. 9485–9499, 2016. https://doi.org/10.1016/j.apm.2016.06.028

[33] Terzi, V. G. "Soil-structure-interaction effects on the flexural vibrations of a cantilever beam", Applied Mathematical Modelling, 97, pp. 138–181, 2021. https://doi.org/10.1016/j.apm.2021.03.045

[34] Terzi, V. G., Manolis, G. D. "Model reduction for structural health monitoring accounting for soil-structure-interaction", Structure and Infrastructure Engineering, 17(6), pp. 779–791, 2021. https://doi.org/10.1080/15732479.2020.1768272

[35] Huergo, I. F., Hernández, H. "Coupled-two-beam discrete model for dynamic analysis of tall buildings with tuned mass dampers including soil–structure interaction", The Structural Design of Tall and Special Buildings, 29(1), e1683, 2020. https://doi.org/10.1002/tal.1683

[36] Huergo, I. F., Hernández-Barrios, H., Patlán, C. M. "A continuous-discrete approach for pre-design of flexible-base tall buildings with fluid viscous dampers", Soil Dynamics and Earthquake Engineering, 131, 106042, 2020. https://doi.org/10.1016/j.soildyn.2020.106042

[37] Araz, O., Elias, S., Kablan, F. "Seismic-induced vibration control of a multi-story building with double tuned mass dampers considering soil-structure interaction", Soil Dynamics and Earthquake Engineering, 166, 107765, 2023. https://doi.org/10.1016/j.soildyn.2023.107765

[38] Tong, F., Christopoulos, C. „Insights on Higher-Mode Effects in High-Rise Buildings with Flexible Base Rotational and Translational Restraints: A Theoretical Study Using a Continuum Beam Analogy", Journal of Earthquake Engineering, 27(2), pp. 314–339, 2023. https://doi.org/10.1080/13632469.2021.2001394

[39] Meza Fajardo, K. C., Papageorgiou, A. S. "Ductility demands of tall buildings subjected to base rocking induced by Rayleigh waves", Earthquake Engineering Structural Dynamics, 48(10), pp. 1174–1194, 2019. https://doi.org/10.1002/eqe.3179

[40] Ferretti, M., D'Annibale, F., Luongo, A. "Buckling of tower buildings on elastic foundation under compressive tip forces and self-weight", Continuum Mechanics and Thermodynamics, 35(3), pp. 799–819, 2023. https://doi.org/10.1007/s00161-020-00911-2

[41] Computers and Structures, Inc. "SAP2000 – Integrated Software for Structural Analysis and Design (Version 24)", [computer program] Available at: https://www.csiamerica.com/products/sap2000 [Accessed: 29 September 2025]